Large Clusters and Colloids. Metals in the Embryonic State

Günter Schmid

Institut für Anorganische Chemie, Universität Essen, D-4300 Essen 1, Germany

Received January 23, 1992 (Revised Manuscript Received August 21, 1992)

Contents

I. Introduction

If a metal particle with bulk properties is reduced to a size of a few dozen or a few hundred atoms, the density of states in the valence band and the conductivity band, respectively, decreases to such an extent that the electronic properties change dramatically.

One question dominates all others: how small does a metal particle have to be so that typical bulk properties (Figure 1a) like conductivity, magnetism etc. begin to disappear, or in other words, when the quasi-continuous density of states is replaced by a discrete energy level structure, with average level separation comparable to or larger than e.g. the thermal energies found experimentally (Figure 1b)? The situation in small molecular clusters is simple. Three metal atoms, for instance, form energetically well-defined bonding and antibonding molecular orbitals (Figure 1c). However, the main point of interest is to be seen in the transition from that in Figure 1a to Figure 1b or vice versa. This quantum size effect can also be demonstrated in another way: if the number of electronic dimensions in a bulk system is reduced from 3 to 2, a so-called quantum well is formed. The electronic one dimensionality leads to a quantum wire, whereas dimension zero results in a quantum dot. On the way from a three-dimensional to a zero-dimensional system the density of states will continuously decrease. In practice, a quantum dot has a dimension of a particle containing hundreds or thousands of atoms. It is of great importance that electrons, trapped in such a particle must have discrete energy levels.

The study of these quantum size effects is a challenge for chemists, physicists, and material scientists. The realization of quantum wires, or even of quantum dots, of uniform size and structure might open the door to multiple switches. These could enable new generations of computers with extremely high capacities. Novel minilasers, based on quantisized particles, could lead to optoelectronic switches, working simultaneously by photons and electrons.

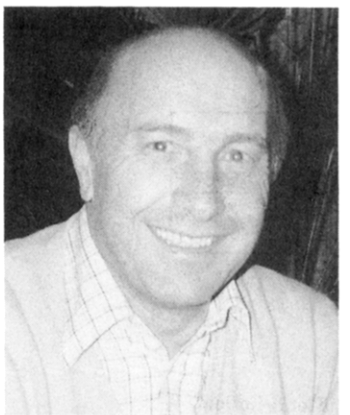

Günter Schmid was born in Villingen, Germany and studied chemistry at the University of Munich. He received his Diploma in 1962 and his Doctor's Degree in Inorganic Chemistry in 1965, both at the University of Munich. In 1966 he moved to the University of Marburg, Germany and finished his Habilitation in 1969. 1971 he got a professorship at the University of Marburg and then he moved to the University of Essen, Germany where he became the director of the Institute for Inorganic Chemistry (1977). His main research interests include the synthesis and investigation of large transition metal clusters and colloids, heterogeneous catalysis, and the investigation of boron-nitrogen disturbed arenes and alkenes as complex ligands.

Clusters as quantum dots are described as follows: They must be fixed, isolated, and regulated in such a way that every quantum dot is embedded into a material with a band gap larger than its own to enable quantum inclusions. Many scientific groups are engaged in achieving this goal. This review will elucidate aspects of the synthesis of large ligand-stabilized clusters and colloids, their characterization, physical properties, and the present situation in heterogeneous catalysis.

It seems useful to think about the application of clusters and colloids as quantum dots. As mentioned above, to enforce quantum inclusions, clusters must be embedded into materials with a larger band gap. In principle, various possibilities seem available. Some groups try to generate quantum dots from semiconductor materials like CdSe in zeolite cages[1] or other hosts like silicate glasses, NaCl, or ZnS.[2,3] The surface coverage of CdSe clusters by organic moieties results in a kind of inverse micelles and gives rise to capped quantum particles.[4] Polymers have also been used as a matrix.[5] More elegant experiments generate quantum dots by lithography. The use of lithographic and epitactic procedures to construct quantum machines and miniaturized lasers is a very promising method in the future.[6,7] However, the use of chemically prepared clusters as quantum dots was recently realized and led to the first tunneling resonance resistance (TRR)[8] (see section V).

0009-2665/92/0792-1709$10.00/0

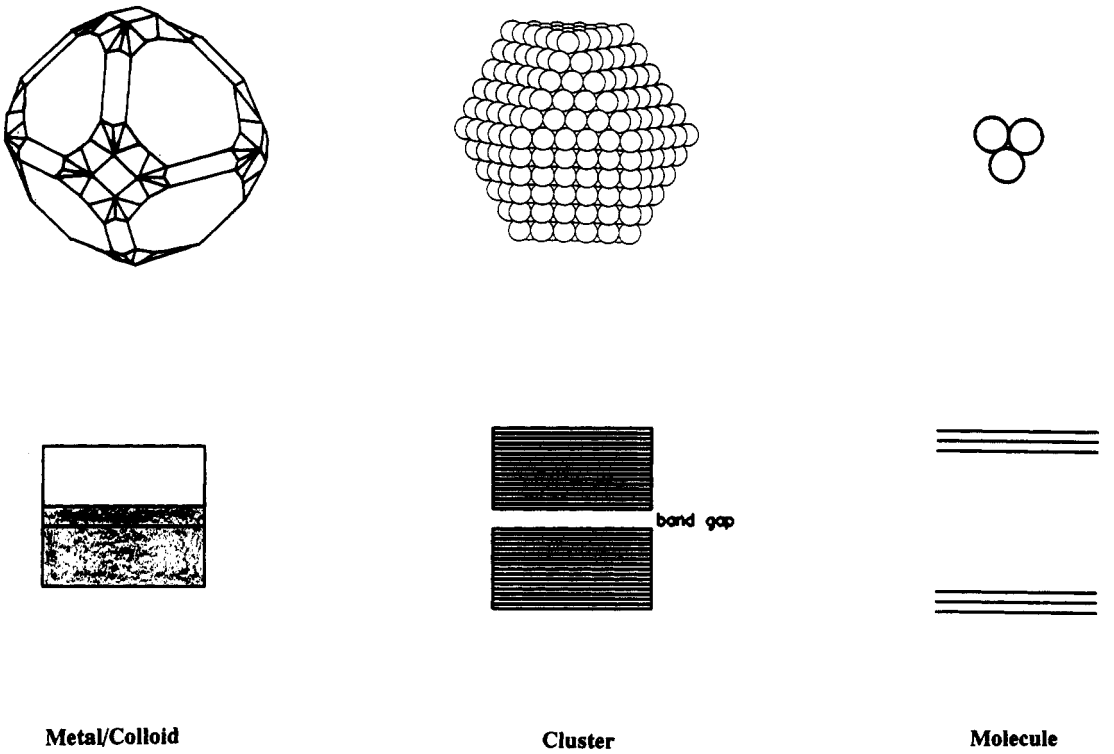

Figure 1. Illustration of the electronic states in (a) a metal particle with bulk properties and its typical band structure, (b) a large cluster of cubic close-packed atoms with a small band gap, and (c) a simple triatomic cluster with completely separated bonding and antibonding molecular orbitals.

The aforementioned experiments, e.g. using semiconductors such as CdSe, may be accompanied by the disadvantage of a substantial size distribution. This problem has not yet been solved. As will be shown in this review, the problem of size distribution of ligand-stabilized transition metal clusters has been solved partially, although not completely as yet.

However, for chemists a completely different field of application for clusters and colloids is relevant and the problem of size distribution is less important: this is the application in catalysis. Special attention shall be directed to the problem, whether the transition from a to b or vice versa in Figure 1 can be observed by studying the physical properties of clusters of different size. To answer this it is necessary, starting from the bulk situation, to reduce the particle size step by step until the bulk properties give way to typical molecular behavior. On the way to this situation we should observe a special size range where the energy-level structure can no longer be treated as quasi-continuous. This continuous reduction of particles of the same kind of atoms does not seem to be practically possible. So, we have to content ourselves with the clusters of different metals described previously. However, these clusters do seem suited for determining the approximate point of the bulk → cluster transition for metal-protected systems.

Another problem should be pointed out, if small particles are to be studied: the smaller a metal particle is, the larger its fraction of surface atoms becomes. Non-protected, naked clusters, not suited for practical purposes, possess surface atoms, which are coordinatively highly unsaturated. They interact only with atoms inside the particle and have free valences outside. So, their electronic contribution to the behavior of the particle is different from that of the inner atoms which are fully coordinated. Surface atoms will be even more distinguishable from inner ones, if they are ligated. As we know from complex chemistry, the interaction of the metal atoms with ligands leads to significant changes in the orbital energies. So, we have to distinguish between the total number of metal atoms forming the complete cluster and the inner atoms, exclusively with other metal atoms as neighbors. The distinction becomes more important the smaller a cluster is. For instance, a dense-packed cluster of 13 atoms has 12 surface atoms, but only one central atom. A two-shell cluster consisting of 55 atoms has a "metallic" nucleus of 13 atoms, whereas the outer shell consists of 42 atoms. Generally, the nth shell includes $10n^2 + 2$ atoms. As we will see in the following, there are many indications that, when regarding the transition to bulk behavior with increasing size, we should consider the inner metal atoms and not the total number of metal atoms. Ligand-free clusters would definitely behave different, but physical investigations of uniform naked clusters are limited so that comparisons between naked and ligand-stabilized clusters of the same size do not seem possible.

II. The Way to Ligand-Stabilized Colloids and Clusters

A. Colloids

1. Gold

We shall begin with particles >10 nm, usually called colloids. Of course, the transition to the smaller clusters is indistinct and not well defined. The metal, which has been investigated comprehensively with respect to its colloidal behavior, is gold. Gold sols are easy to prepare and are characterized by an attractive color which can vary from ruby red through purple to blue.

The beautiful red color of the so-called ruby glass, caused by uniformally dispersed gold colloids, has been known since the end of the middle ages. Purple of Cassius has been used for various things, for instance as precious pigment. The reason for the intensive color was discovered by M. Faraday in 1858. Later, gold colloids have been used especially in biology, and this range of application has intensified up to now. Colloidal gold, labeled to various biological materials like lectins, antibodies, antigens, enzymes, or lipoproteins enable these systems to be observed by transmission or scanning electron microscopic methods. Bright-field, dark-field, and fluorescent microscopy also use gold-labeled materials as well as back-scattered electron imaging with secondary electron signals or photoelectron microscopy.[9]

In principle, metal colloids can be generated in two different ways: by dispersion of larger particles (dispersion method) or by condensation of smaller units (reduction method). Among the dispersion methods only the electric dispersion of metal electrodes in water is of importance. Sols, prepared by this method, are rather unstable and consist of particles with a wide size distribution. A better strategy to generate uniform particles is to use chemical methods such as by the reduction of metal salts in solution. Chemically prepared metal colloids are only stable in solution, as they are protected by solvent molecules and electric charges, preventing coagulation. Addition of so-called protecting colloids to the solution of a metal sol leads to a better stabilization. Synthetic macromolecules like poly(vinyl alcohol),[10-12] poly(vinyl pyrrolidone),[10] copolymers of vinyl alcohols and *N*-vinyl pyrrolidone,[13] cyclodextrins,[14] colloidal silicic acid,[15] and others have been used. The protective effect of these compounds is due to the fact that either the smaller colloids are fixed on the much larger protecting colloids or that the protecting molecules cover or envelope the metal particles.

These stabilizers keep the colloidal metal in solution and reduce the sensitivity toward other electrolytes. However, none of these methods can be used to isolate metal colloids. Indeed, such stabilized colloidal solutions allow numerous physical investigations. However, the main part of the mass consists of the matrix material and not of the colloids themselves. To make metal colloids available like "normal" chemical compounds, i.e. in order to isolate them in a solid state and to make them soluble in any concentration, a completely different way to stabilize colloids must be found. Such a stabilization has been realized successfully by low-molecular complexing agents. The stabilization of rhodium colloids by $OP(C_6H_4SO_3Na)_3$ was first reported in 1988;[16] however, no information was given about the nature of these colloids.

In particular, gold colloids can be prepared very easily by the reduction of diluted aqueous solutions of $HAuCl_4$ with citric acid[17] or trisodium citrate.[16,18-23] If trisodium citrate is used, a very narrow size distribution is observed with standard deviations of only 10%. Variation of the experimental conditions allows the synthesis of particles with diameters between 14 and 900 nm. Colloids of a distinct size became available by the so-called germ-growth method.[16,24] For this purpose one starts with a smaller colloid, e.g. 18 nm, available by the citrate method. In a second reduction step a certain amount of additional $HAuCl_4$ is reduced by hydroxylammonium chloride. The 18-nm colloidal particles are now used as a nucleus to germinate and grow the colloids to the calculated size. The diameter of the colloid to be obtained (d) can be calculated by the following formula:

$$d = d_0 \sqrt[3]{\frac{n_i + n_m}{n_m}}$$

where d_0 = particle diameter in the solution of the starting nucleus and n_i, n_m = quantity of the ionic and metallic gold, respectively. By the addition of water-soluble phosphines such as $Ph_2P(m\text{-}C_6H_4SO_3Na)$ or better $P(m\text{-}C_6H_4SO_3Na)_3$ such gold colloids can be stabilized to such an extent that they can be isolated as solid materials. They can then be dissolved in water in any concentration forming blood-red solutions.[25,26] On smooth glass or paper surfaces such solutions dry to give metallic looking gold mirrors. On porous materials the red color of the colloids is preserved.

There is a disadvantage of the sulfonated phosphine ligands: they hydrolyze in water slowly to give triphenylphosphine, or they are oxidized by air to the phosphine oxides.[27] Both products are unable to stabilize gold colloids in aqueous solution.

However, under exclusion of air and moisture, ligand stabilized colloids can be stored for unlimited time. Figures 2 and 3 show some typical details of phosphine-protected gold colloids.

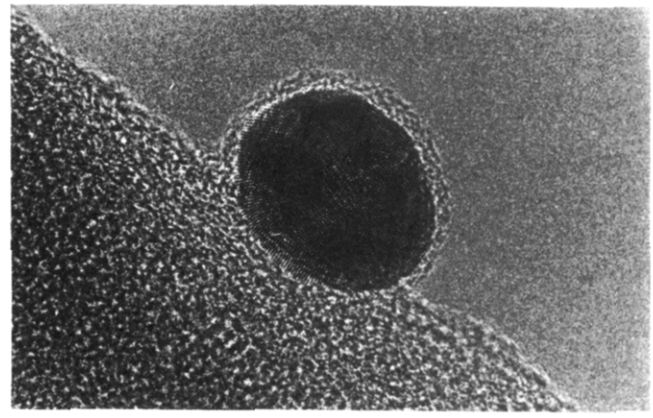

Figure 2. A single, polycrystalline gold colloid of about 13.2 × 10.5 nm. The ligand shell, consisting of a double layer of $P(m\text{-}C_6H_4SO_3Na)_3$ molecules, can be clearly observed.

Figure 2 shows an image of a single, $P(m\text{-}C_6H_4SO_3Na)_3$-stabilized gold colloid, obtained by means of high-resolution transmission electron microscopy (HRTEM).[28] One recognizes the polycrystalline structure of the elliptic particle, with dimensions of about 13.2 × 10.5 nm. Normally most of the microscopically observed gold colloids are polycrystalline, but monocrystalline particles can also be observed. HRTEM investigations as well as X-ray reflections in powder diffractograms prove that the atomic packing of the metal atoms corresponds with that in the bulk, that is they display the fcc structure. Moreover, a 1.0–1.2-nm thick noncrystalline shell, enveloping the colloid, can be observed in Figure 2. The thickness of this ligand shell corresponds precisely with a double layer of the phosphine ligand, as we know from an X-ray analysis of $Ph_2P(m\text{-}C_6H_4SO_3Na)$.[29] This double layer of phos-

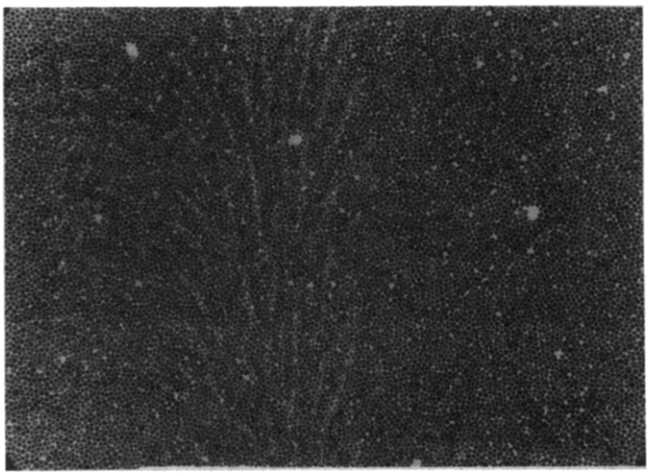

Figure 3. A close-packed monolayer of 14-nm gold colloids, protected by P(*m*-$C_6H_4SO_3Na)_3$ ligands.

phine ligands can also be deduced from Figure 3, where a two-dimensional dense-packed monolayer of 14-nm gold colloids, stabilized by the same ligand, is shown. The average distance between the particles agrees with four monolayers of the phosphine. Due to their ionic substituents, the phosphine ligands prevent coalescence to a large extent. However, during the experiment itself the portion of aggregates increases by the intensive electron irradiation in the microscope, which tends to force the ligands off.

If gold colloids are deposited from an extremely dilute solution, very characteristic patterns can be observed. This kind of deposition can best be described by Monte-Carlo simulations.[25] Figure 4a shows such a typical pattern of 36-nm ligand-stabilized gold colloids. In Figure 4b it is illustrated how such a pattern may be formed.

2. Palladium and Platinum

Besides gold, the easy formation of palladium and platinum colloids is also known.[30-34] In principle, the synthetic routes are the same as for gold colloids. The reduction of H_2PdCl_4 and H_2PtCl_6, respectively, with trisodium citrate leads to brown-colored particles, which can best be stabilized by *p*-H_2N-$C_6H_4SO_3Na$. Like the Au colloids, the Pd and Pt colloids can then be isolated in solid state and redissolved in any concentration in desalinated water. These colloids also form metallic looking mirrors when deposited on smooth surfaces from solutions. The Pd colloids as well as the Pt colloids have fcc structures as do the bulk metals. This can easily be shown by X-ray powder diffractions. HRTEM studies of Pd colloids show that they are formed in a similar narrow size distributions as the Au colloids. In contrast, the situation for platinum colloids is not as good. Figure 5a shows *p*-H_2N-$C_6H_4SO_3Na$-stabilized Pt colloids. The filamentary looking pattern is very characteristic. A magnified section of the same sample is shown in Figure 5b. The particles are much more irregular and have a large size distribution. The particle size in Figure 5b varies between 2 and 4 nm. This size agrees well with literature data.[30-36] However, the monodispersive character, which has been reported by several authors[33,35] was not observed by us. It may be that their findings were based on electron micrographs whose resolution was too low.

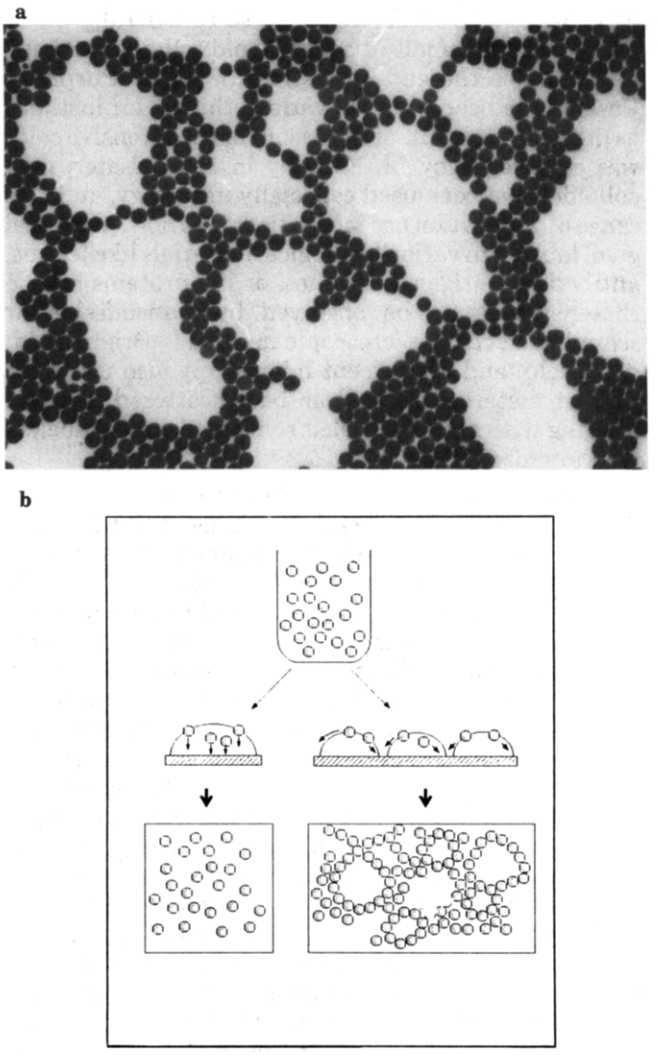

Figure 4. (a) A typical pattern of 36-nm ligand-stabilized gold colloids, deposited from a very dilute solution and (b) illustration of the formation of the experimentally observed pattern by Monte Carlo simulations. Colloidal particles in very small droplets move on the surface toward the peripheries and do not precipitate uniformly as shown in the left example.

Bimetallic particles find increasing interest not only in catalysis, but also as models for the study of the formation of alloys. They can be divided into two classes: Alloylike colloids consist of a homogeneous mixture of two metals with colloidal distribution, and colloids with an inner nucleus of one metal, which is covered by a layer of the second metal. Both types have already been described.[34,37] The alloylike colloids are prepared by coreduction of two metal salts in solution. Bimetallic colloids constructed in layers are obtained by using the germ-growth method: the germ sol is covered by the second metal during a second reduction step. Bimetallic colloids with a layered structure can be stabilized like the monometallic species with appropriate ligands. Our investigations have been focused on the systems Au/Pt and Au/Pd. If Pd or Pt form the outer shell, *p*-H_2N-$C_6H_4SO_3Na$ is best suited for the stabilization. In the case of a gold envelope, P(*m*-$C_6H_4SO_3Na)_3$ is used to protect the particles.[24] For instance, 18-nm Au colloids are used as germs to be covered with a calculated layer of Pt. The subsequent stabilization with *p*-H_2N-$C_6H_4SO_3Na$ leads to brown isolable colloids.[38] Only HRTEM shows the real nature of such particles. In Figure 6 two typical Au/Pt colloids

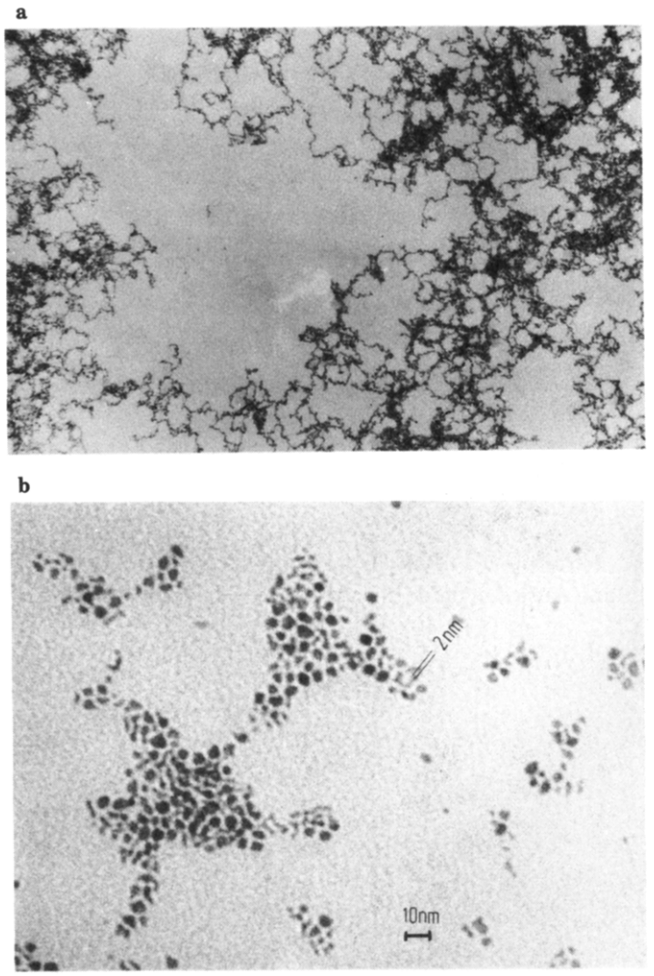

Figure 5. (a) Platinum colloids, stabilized by p-H_2N-$C_6H_4SO_3Na$ and (b) the same colloids in a magnified section. The size distribution varies between ca. 2 and 4 nm.

are shown. They have about the same size, but they look like an agglomerate. The energy dispersive X-ray microanalysis (EDX) shows clearly that the peripheral areas consist of about 5-nm particles of platinum, covering the inner gold core. Obviously the formation of this platinum envelope is preceded by the generation of the 5-nm particles, which then attach to the surface of the 18-nm gold colloids. Laser-optical diffractograms of the 35-nm Au/Pt particles show that they consist of two different types: in colloid A all Pt particles have the same crystallographic orientation, whereas B shows random orientation for the small Pt particles. There is probably a relation between the structure of the inner gold nucleus and the structure of the whole particle. We shall come back to this problem when we discuss the Au/Pd combination. The reason why the platinum does not grow as a compact shell on the gold surface is not completely understood. Presumably it is to be found in the broad miscibility gap, which is found for the Au/Pt system between 2% and 85% of Au. In contrast to this observation, it has been reported that gold and platinum form alloylike colloids in various mixing proprotions if their salts are reduced simultaneously.[34]

In contrast to the Au/Pt system, gold and palladium are miscible in any ratio. This is also true for Au/Pd colloids. HRTEM investigations of ligand-protected Au/Pd colloids prove the existence of two kind of

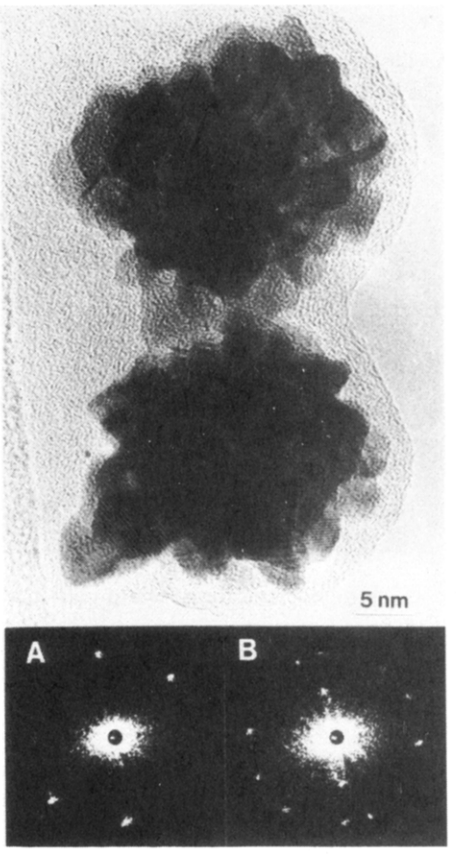

Figure 6. Two different types of Au/Pt colloids with intergranular structures. The inner Au cores are covered by ca. 5-nm Pt particles. The optical diffractogram of colloid A proves the same crystallographic orientation of all Pt particles. B shows a random orientation for the Pt particles.

particles as found in the Au/Pt case, but both kinds look homogeneous.

Again, the EDX analysis of both kinds of particles in Figure 7a,b shows that the peripheral parts consist solely of palladium. As calculated from the preparative results, 17 atomic % of Au and 83 atomic % of palladium are found.[37]

While the Pd atoms in particle a are arranged completely monocrystalline, b shows a polycrystalline character. The optical diffractogram confirms the different symmetries. As in the Au/Pt system, these different structures can be traced back to the structure of the gold colloid. Monocrystalline Au nuclei might give rise to the formation of type a in Figure 7, whereas polycrystalline nuclei cause type b.[37]

An impressive image of a monocrystalline Au/Pd colloid is shown in Figure 8.[39]

B. Clusters

Due to the lack of appropriate compounds, we have to make a big step now on the way from large to small particles, namely from 15–40-nm colloids to 2–4-nm clusters. The synthesis of these species is similar to that of colloids: a metal salt, in this case palladium(II) acetate, is reduced in aqueous solution in the presence of the protecting ligand phenanthroline.[40] Hydrogen is used as a reducing agent. The resulting Pd clusters are extremely sensitive to oxygen. To prevent uncontrolled reactions, they are carefully oxidized in solution by oxygen in order to cover those surface atoms, which

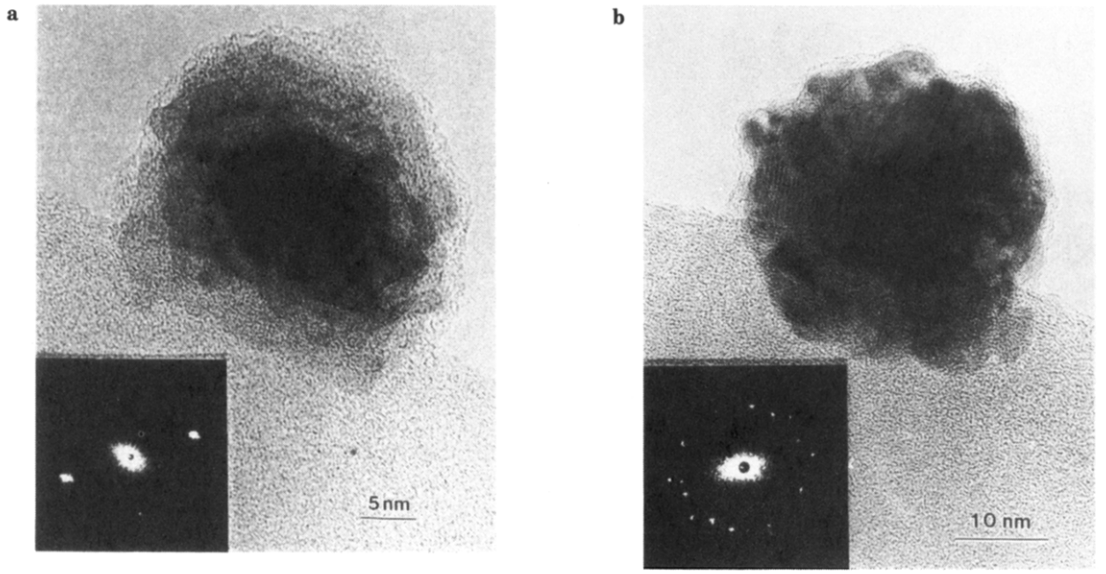

Figure 7. (a) A monocrystalline Au/Pd colloid and (b) polycrystalline Au/Pd colloid, in contrast to Au/Pt colloids with a smooth surface.

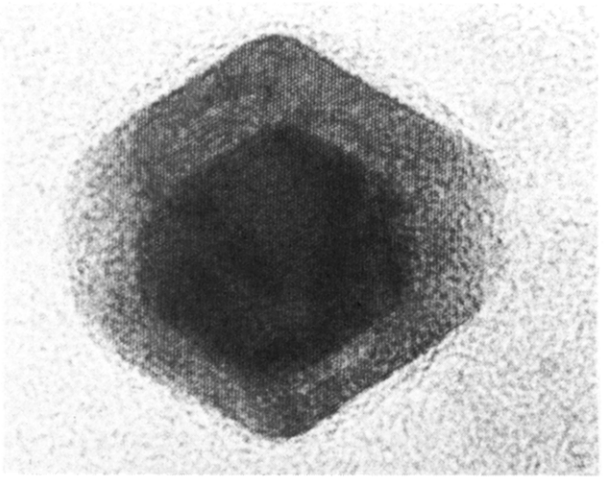

Figure 8. A monocrystalline Au/Pd colloid. EDX analyses prove the dark inner part to consist of Au, the outer part of Pd.

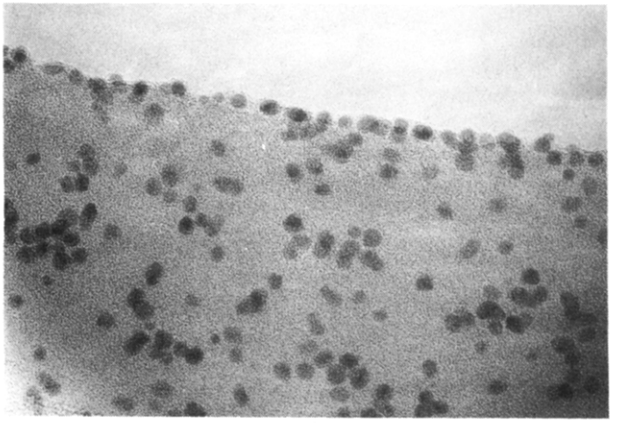

Figure 9. A mixture of phenanthroline- and oxygen-covered Pd clusters, consisting mainly of seven- and eight-shell structures with 31.5- and 36.0-Å diameters.

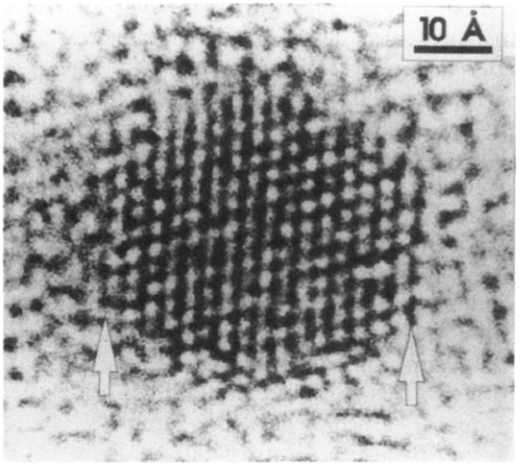

Figure 10. A single eight-shell cluster in high resolution with fcc structure.

are not coordinated to phenanthroline, so that they can be handled in air. The reaction of palladium(II) acetate with hydrogen leads to three different cluster sizes: One fraction mainly consists of clusters with 31.5 and 36.0 Å in diameter, which could not be separated from each other. In the terminology of the full-shell concept these diameters correspond with seven- and eight-shell clusters. This concept describes a cubic or hexagonal close-packed structure consisting of one central atom, which is surrounded in the first shell by 12 atoms, in the second shell by 42 atoms, or in principle by $10n^2 + 2$ atoms in the nth shell. If the 31.5- and 36.0-Å particles were perfect in structure (in practice this is not normally the case) they would consist of 1415 and 2057 atoms, respectively. In contrast to the large colloids, these clusters give HRTEM images, which show their predominant monocrystalline character. Figure 9 shows a section of an area, covered with these clusters. In Figure 10 a single, almost perfect eight-shell cluster of cuboctahedral fcc structure is shown.

Another product of the above mentioned experiment is a relatively well defined five-shell cluster of the idealized formula $Pd_{561}phen_{36}O_{200\pm20}$.[41,42] It is best separated from the seven- and eight-shell clusters by fractionating centrifugation. In Figure 11 a larger number of these five-shell clusters is imaged.

Palladium clusters of the same size were already described by Moiseev et al. in 1985.[43] X-ray powder diffractions of five-, seven-, and eight-shell Pd clusters

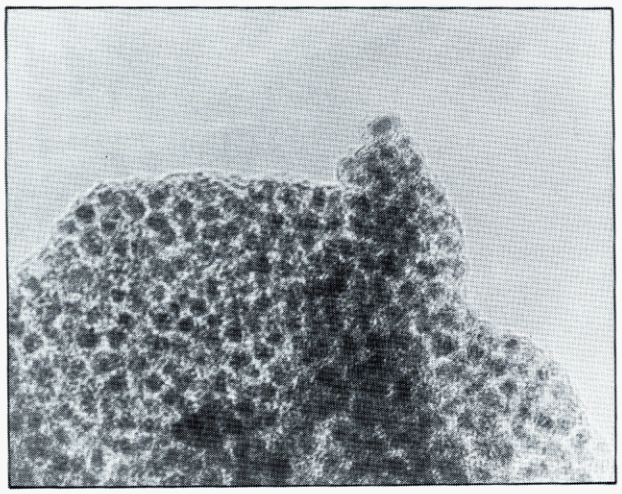

Figure 11. A larger area with five-shell Pd clusters.

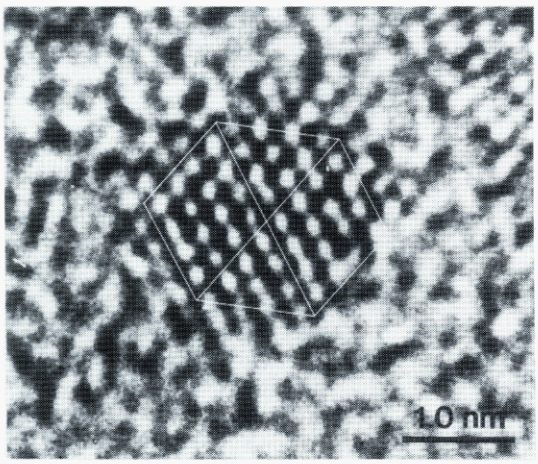

Figure 12. A HRTEM image of a Pt_{309} cluster molecule in (110) direction with fcc structure.

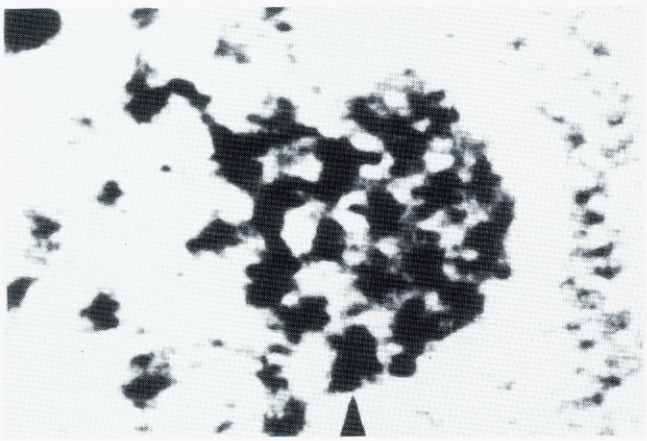

Figure 13. A single Pt_{55} cluster with fcc structure in atomic resolution (110 direction).

indicate in every case that they have fcc structure like the bulk state. This has already been shown by HRTEM.

The same synthetic principle can be used to prepare four-shell platinum clusters. The reduction of platinum(II) acetate in aqueous solution in the presence of phen* with following oxidation by O_2 gives Pt_{309}-phen*$_{36}O_{30\pm10}$.[44] HRTEM investigations prove an almost perfect uniformity in size and shape.

Figure 12 shows a HRTEM image of one of these cluster molecules. It has indeed a perfect fcc structure

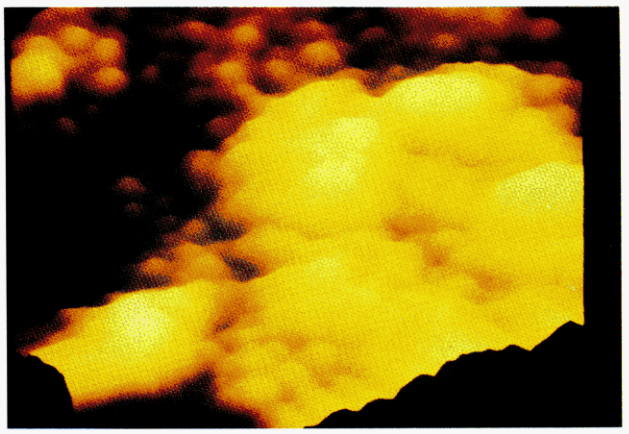

Figure 14. STM image of $Pd_{561}phen_{36}O_{200}$ clusters. The spheric looking molecules still possess their ligand shell.

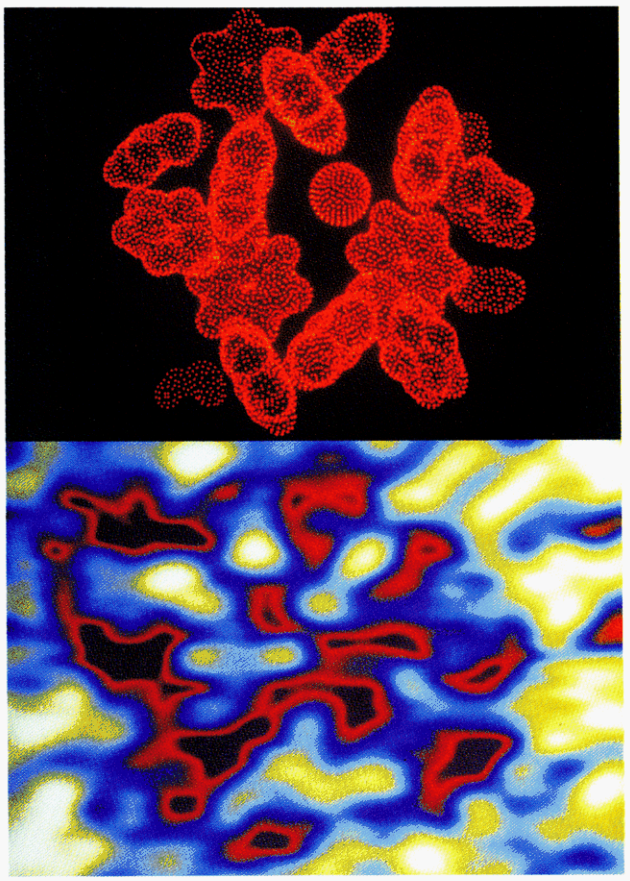

Figure 15. (Top) A computer-simulated "two-dimensional" electron-density image of $Au_{55}(PPh_3)_{12}Cl_6$; in the center of the image a Cl atom is to be seen and (bottom) STM image of a $Au_{55}(PPh_3)_{12}Cl_6$ molecule, showing mainly the electron density of the phenyl rings and of a chlorine atom. The similarities between the top and bottom are evident.

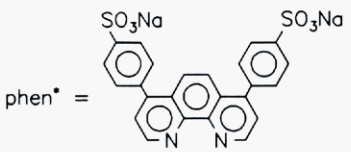

with the outer geometry of a cuboctahedron.

Finally, the series of the clusters under discussion ends with compounds of the type $M_{55}L_{12}Cl_x$ (M = Rh, Ru, Pt, Au, L = PR_3, AsR_3, x = 6, 20). They are formed by reduction of appropriate metal salts, not by hydrogen in aqueous solution, but by B_2H_6 in organic solvents.[45-47]

The electron microscopic imaging of these clusters with extremely high resolution occasionally succeeds, as can be seen from Figure 13. It shows a two-shell Pt_{55} cluster with its typical fcc structure as found in the bulk metal. Under the influence of the high-energy density of the 400-keV electron beam, these very small metal particles rapidly change structure and size.[48] The clusters begin to move on the grid surface, then they coalesce and form larger clusters and aggregates. These events allow the observation of highly interesting processes such as rearrangements, crystal growth, column hopping, etc. by microscope. These processes shall however not be discussed in this review.

Initial experiments to produce pictures of single clusters by means of the scanning tunneling microscopy (STM) appear very promising. Figure 14 shows first results of the imaging of the $Pd_{561}phen_{36}O_{200}$ cluster with almost "molecular resolution".[49,50]

The method may be well suited to determine the cluster size including the ligand shell. It would be interesting to see what kind of image one would get, with increased resolution. Of course, it cannot be expected to reach the same atomic resolution, as is known from smooth surfaces for instance of graphite, gold, etc. Initial attempts have been made to obtain images of $Au_{55}(PPh_3)_{12}Cl_6$ by STM with a better resolution than shown in Figure 14, and it is difficult to explain all details. If a single cluster molecule is scanned by the tip of the STM microscope, it can be expected that a kind of a two-dimensional electron density profile of the ligands results. Computer models of such representations can be compared with experimental images. In Figure 15 the simulated computer model (top) and the STM image (bottom) of a cluster molecule is shown. Figure 15a was produced by rotating a dot electron model of $Au_{55}(PPh_3)_{12}Cl_6$ into various positions by use of XP-Software (SHELXTL-Plus). That position which matched the STM picture the most was stopped and the hidden parts which are not detected by the STM technique were extinguished. A reasonable agreement between the top and bottom of Figure 15 can be recognized. So HRTEM and STM complement each other in an ideal manner.[51,52]

HRTEM gives information about size and structure of the cluster nucleus, whereas STM enables the imaging of the ligands. Together one can get a reliable image of such large clusters.

A gold cluster $[Au_{39}(PPh_3)_{14}Cl_6]Cl_2$, which is close to the Au_{55} cluster in size, was recently crystallized and therefore was able to be investigated by X-ray methods. It consists of a hexagonal antiprismatic cage, coordinated by 14 PPh_3 ligands and 6 chlorine atoms.[53] In contrast to some bimetallic AuAg clusters, e.g. $[(p\text{-tolyl})_3P]_{10}Au_{13}Ag_{12}Cl_8^+$,[54] which consist of interpenetrating icosahedra, the monometallic Au_{39} cluster elucidates the tendency of larger metal assemblies to form close-packed structures.

A series of large transition metal clusters containing ligands from the main groups five and six could also be investigated by means of X-ray analyses so that structural details have been obtained.[55] A general route, consisting of the reaction of various simple metal halide complexes with silylated group five and group six elements as $E(SiMe_3)_2$ (E = S, Se, Te) and $E'R(SiMe_3)_2$ (R = Ph, Me, Et; E' = P, As, Sb), leads to numerous nickel and cobalt clusters with 4 up to 34 metal atoms. The molecular structure of $Ni_{34}Se_{22}(PPh_3)_{10}$ is shown in Figure 16.

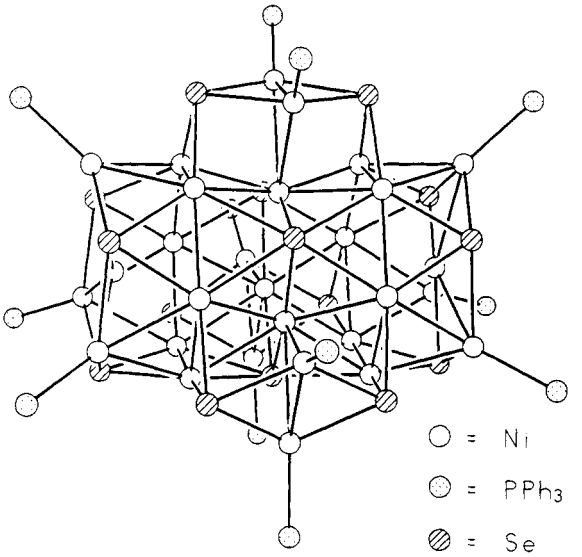

Figure 16. The molecular structure of $Ni_{34}Se_{22}(PPh_3)_{10}$.

Whereas the structures of various smaller chalcogenide clusters in principle consist of condensed octahedra, $Ni_{34}Se_{22}$ is characterized by a novel structural principle: It contains a central pentagonal antiprismatic Ni_{14} core to which five Ni_4 butterfly units are added. Some fascinating large copper clusters have recently been described by the same group.[56] $Cu_{36}Se_{18}[P(t\text{-}Bu)_3]_{12}$ and $Cu_{70}Se_{35}(PEt_3)_{22}$ are obtained from CuCl and $Se(SiMe_3)_2$ in the presence of phosphines. The structures of these clusters are complicated and will not be discussed here. However, it should be noticed that these clusters may be seen as molecular precursors of binary copper selenides. Indeed, if heated to >160 °C, PEt_3 is eliminated and the formation of β-Cu_2Se via an unknown phase is observed. The function of these chalcogenide clusters as metal selenide precursors can be compared with the above-mentioned metal full-shell clusters as precursors for metal formation.

A series of As- and Sb-bridged palladium clusters results from the reaction of $PdCl_2(PPh_3)_2$ with $As(SiMe_3)_3$ and $Sb(SiMe_3)_3$.[57,58] $Pd_9As_8(PPh_3)_8$, $Pd_9Sb_6(PPh_3)_8$, and $Pd_{20}As_{12}(PPh_3)_{12}$ are all characterized by chalcogenide bridges between the Pd atoms. The Pd_{20} cluster nucleus consists of a Pd_8 cube, each vertex of which is bridged by a $PdPPh_3$ group.

Finally, some large carbonyl clusters should be mentioned, especially because some of them have been studied by physical and theoretical methods.

The story of high nuclearity carbonyl clusters culminated in the synthesis of $[Pt_{26}(CO)_{32}]^{2-}$,[59] $[Pt_{38}(CO)_{44}H_2]^{2-}$,[59] and $[Ni_{38}Pt_6(CO)_{48}H]^{5-}$.[60] The structural characteristics of all these carbonyl clusters follow the principle of closest packings. The Pt_{26} cluster shows a hcp structure with the layer sequence ABA, whereas the Pt_{38} metal nucleus consists of ccp-packed metal atoms. Its structure is shown in Figure 17.

This review only considers ligand-stabilized clusters and colloids. Metal particles which have been synthesized by all kind of molecular beam techniques, as well as clusters in cages such as zeolithes cannot therefore be dealt with in this report. Cluster beam

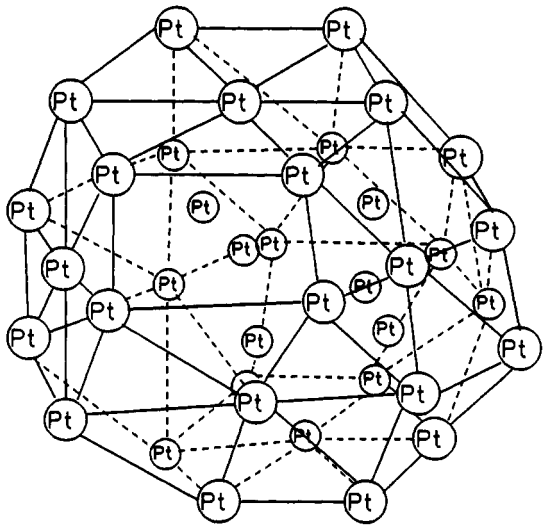

Figure 17. The fcc-packed Pt_{38} cluster nucleus of the $[Pt_{38}(CO)_{44}H_2]^{2-}$ ion.

techniques in general generate naked particles which can be investigated in the gas phase or are deposited on various supports, e.g. for the preparation of catalysts. The present knowledge on this field of cluster chemistry and physics can be ascertained from some recent reviews.[60-63]

III. Properties

A. Physical Properties

If the physical properties of ligand-protected clusters and colloids is to be studied, we must always realize that the ligand shell changes the electronic states of those metal atoms which are linked with the ligand molecules. A ligand-stabilized cluster molecule cannot have the same properties as a particle of the same size without a ligand shell.

The two-shell cluster $Au_{55}(PPh_3)_{12}Cl_6$ is well suited for Mössbauer spectroscopic investigations. The ^{197}Au Mössbauer spectra of this cluster have therefore been studied very intensively.[64]

The spectra of $Au_{55}(PPh_3)_{12}Cl_6$ show contributions from four different types of Au atoms (Figure 18): 13 inner atoms, forming the nucleus of the cluster, 24 uncoordinated surface atoms, 12 atoms coordinated to the PPh_3 ligands, and 6 chlorine-bonded atoms. This means that not only ligand bearing surface atoms, but also uncoordinated atoms differ characteristically from inner core atoms, forming the "metallic part" of the whole cluster. The chemical shift of the signal caused by the inner Au_{13} nucleus is quite close to that of bulk gold. The temperature dependence of the spectrum is much more pronounced than that of a bulk metallic specimen. Bulk gold shows almost no dependence of temperature below 80 K. The Mössbauer effect gives information on the phonon excitations within the metal particle itself. By means of the Mössbauer data the vibrational parameters and through these the phonon contributions to the low temperature specific heat can be calculated: they are in excellent agreement with the experimental specific heat data. In the specific heat no linear term could be detected, indicating the lack of the electron contribution predicted by the free electron theory of bulk metals. A decisive consequence from

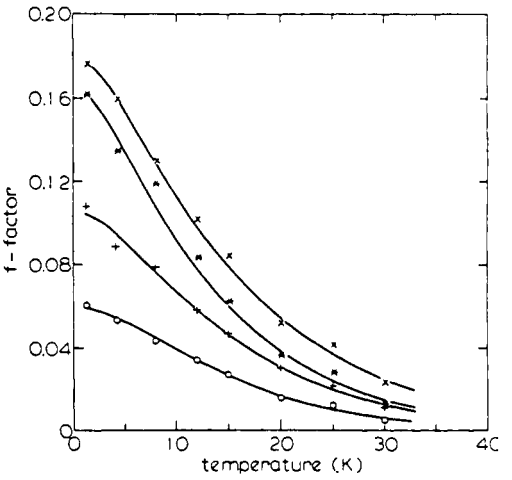

Figure 18. Temperature dependence of the Mössbauer fraction of the four gold sites in $Au_{55}(PPh_3)_{12}Cl_6$: (×) core, (*) Cl bonded, (+) unbonded surface, and (○) PPh_3-bonded Au atoms. The fits, using the product of two Einstein functions, are shown by the solid lines.

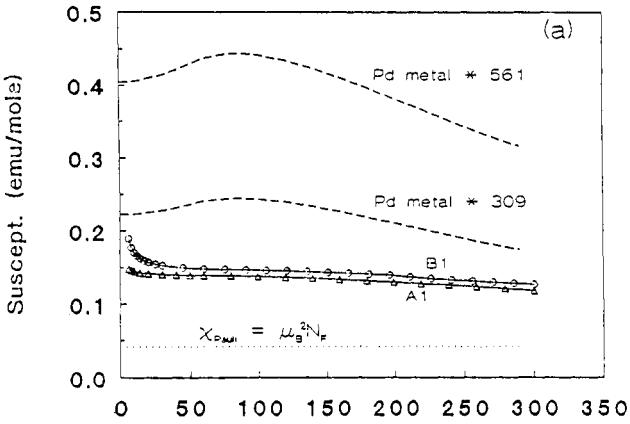

Figure 19. Susceptibility of two different samples of $Pd_{561}phen_{36}O_{200}$ (A1, B1), compared with the bare Pauli susceptibility and with the calculated values for bulk Pd, scaled to Pd_{561} and Pd_{309}.

the Mössbauer investigations is the fact that the Au_{13} cluster nucleus shows a frequency, which is close to the bulk and is remarkably different from that of the other gold atoms. This is one of the first experimental indications that the formation of a metallic state is mainly determined by the cluster nucleus, and not by the surface atoms.

EXAFS studies of $Au_{55}(PPh_3)_{12}Cl_6$[65,66] at 8 K indicate a slightly distorted cuboctahedral structure with a first neighbor Au–Au distance of 2.803 ± 0.01 Å. That is characteristically smaller than in the bulk with 2.878 Å. This contraction can be explained by the Gibbs pressure. The distortion of the cuboctahedron may be due to an anisotropy in the surface stress and probably explains why the higher shells cannot be seen by EXAFS.

A breakthrough in the field of metal formation studies is, without doubt, the result of more recent ^{195}Pt NMR studies on $Pt_{309}phen^*_{36}O_{30}$. Platinum shows one of the largest Knight shifts (K) among all metals. This enables the observation of electronic properties on the way from the molecular to the bulk state. So, NMR experiments with Pt clusters help to establish the minimal number of atoms which is necessary to show "metallic behavior", since a Knight shift is one of the hallmarks of metallicity.

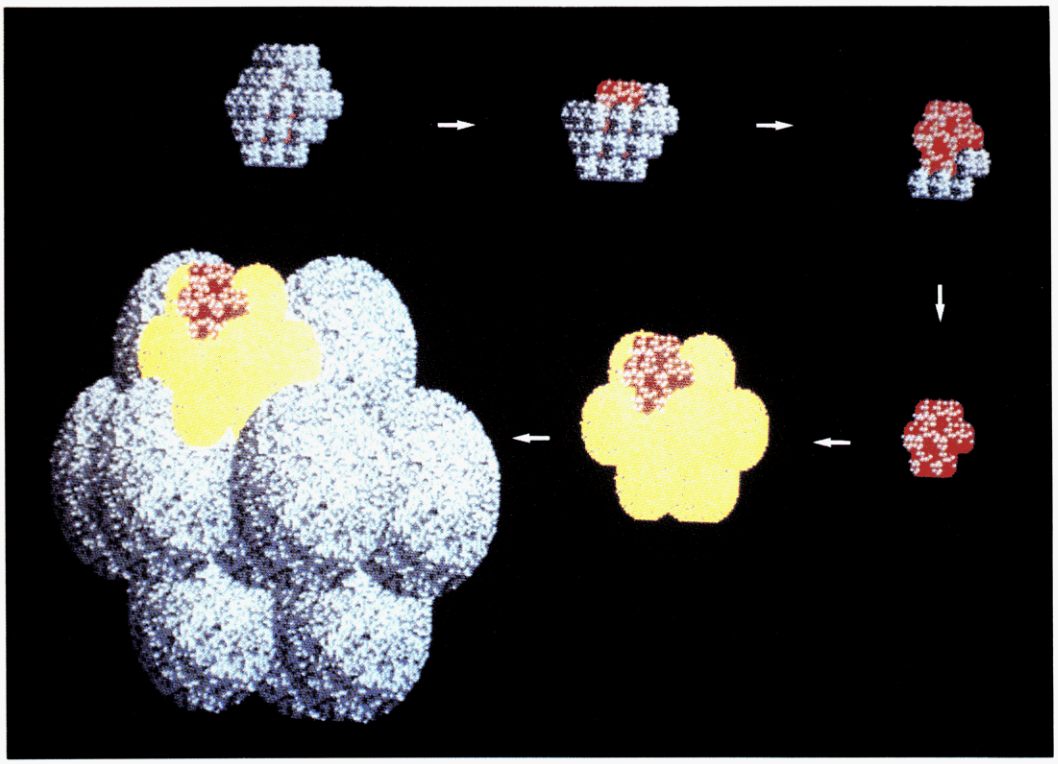

Figure 20. Formalized degradation of M_{55} clusters to $(M_{13})_n$ superclusters (without ligands). The (red) M_{13} clusters aggregate to $(M_{13})_{13}$ (yellow) and to $[(M_{13})_{13}]_{13}$ (blue) particles.

The ^{195}Pt NMR spectrum of $Pt_{309}phen^*_{36}O_{30}$ shows two signals at $H_0/\nu_0 = 1.110$ and 1.096 G/kHz. The analysis of the spin–lattice relaxation time T_1 shows the high-field peak to be caused by Pt spins of the inner atoms, which are in a metallic environment. This is indeed the first observation of metallic behavior in a molecular cluster compound. The low-field peak is due to the surface platinum atoms that are coordinated to the ligand molecules.[67]

The NMR results are supported by magnetic measurements with various cluster types.[68,69] M_{55} clusters of nonmagnetic metals like Au_{55}, Rh_{55}, Ru_{55}, and Pt_{55} show only small susceptibilities. At low temperatures a weak rise in χ can be distinguished. From that one can conclude a small unpaired spin density residing on the cluster. It can be assumed that the effect of ligand coordination to the surface atoms has strong analogies with the crystal field effect on single metal atoms in simple complexes. There, the ligand strength determines if high- or low-spin complexes are formed. The observed small free-spin density in clusters of nonmagnetic metals may have similar reasons. The energy-level structure is significantly influenced by the embedding ligand field if compared with naked particles. So, the ensuing redistribution of the available electrons can be the reason for the observed free-spin density.

In agreement with the results of experimental magnetic measurements of some high-nuclearity Ni clusters[70] theoretical calculations also indicate the developing of a metallic character,[71] better to be observed with Ni instead of Au, Pt, or other metals which are diamagnetic in the bulk state.

The influence of the ligand shell on the susceptibility of a cluster molecule becomes visible at the five-shell cluster $Pd_{561}phen_{36}O_{200}$ the uniformity of which has been controlled by HRTEM. The result from SQUID magnetometry investigations is shown in Figure 19.[56]

The susceptibility values lie characteristically above the calculated free-electron Pauli-spin susceptibility for a metallic cluster of 561 Pd atoms. Furthermore, the behavior of the susceptibility for bulk palladium metal is drawn, scaled to 561 and 309 atoms. As is known, χ for bulk Pd is largely enhanced above the free-electron value (large Stoner enhancement factor). While the values scaled to 561 atoms are still well above the experimentally obtained values of two different specimen, the scaling to 309 atoms brings the susceptibility close to the experimental values. This means that the inner Pd_{309} core of the five-shell cluster shows a bulklike χ behavior, whereas the contributions of the surface atoms is quenched through the ligand effects.

Hence, the susceptibility measurement of $Pd_{561}phen_{36}O_{200}$ again shows that the contribution of the inner core, in this case 309 atoms, is responsible for the cluster properties under discussion. Except for the NMR result of $Pt_{309}phen^*_{36}O_{20}$ this is the second case where bulklike behavior of a ligand-stabilized cluster can be manifested. There is a third indication for a beginning bulk behavior of cluster cores of larger clusters, namely specific heat measurements on $Pd_{561}phen_{36}O_{200}$ at low temperatures.[56] The specific heat below 1 K turns out to contain linear contribution $C = \gamma T$, which can be interpreted as an electronic contribution. The value of γ is found to be about one-third of the value of bulk palladium.

Finally some recent results from optical investigations shall be mentioned. The optical excitation of plasmon polaritons (Mie-resonance) and the complex low-frequency dielectric function indicate that in ligand stabilized Au_{55} clusters the 6s electrons are delocalized, but the transition to the behavior of the metallic gold is not yet completed.[72,73]

In summary, the physical data known to date tell us that ligand-stabilized M_{55} clusters show the beginning of electron delocalization. Moreover, clusters of the

size of Pt_{309} and Pd_{561} already show distinct bulk properties. It should be considered that in both cases the real contributions to metallic behavior come from the inner core atoms, so that our discussions mainly concern M_{13}, M_{147}, and M_{309} atomic particles.

B. Chemical Properties

The chemical properties of large ligand-stabilized transition metal clusters are, strictly speaking, rather limited. This is especially due to their marked tendency to decompose in solution. The partial dissociation of ligands leads to relatively fast aggregation processes via free surface atoms and finally to the precipitation of metal. Therefore, chemical reactions are limited to fast reactions in the ligand sphere. The extent of the decomposition tendency, of course, varies and depends mainly on the kind of ligand.

From experience we know that phosphine-stabilized clusters in organic solvents are much less stable than phen- and phen*-stabilized clusters in aqueous solution. Ligand-stabilized colloids are very sensitive to additional electrolytes.

Extensive ^{31}P NMR investigations on phosphine-stabilized M_{55} clusters in solution have shown that the phosphines are highly fluxional.[74] For instance, $Rh_{55}[P(t\text{-}Bu)_3]_{12}Cl_{20}$ causes only one sharp ^{31}P NMR signal at 68 ppm at room temperature, although ^{103}Rh–^{31}P couplings are to be expected. Due to the high fluxionality of the phosphine ligands all couplings are obviously averaged. The PPh_3 ligands in $Au_{55}(PPh_3)_{12}Cl_6$ are also scrambled. The average contact time of the phosphine molecules with the gold surface atoms is 3 μs. In one case it enabled the use of the weak bond between PPh_3 and the gold atoms for substitution reactions. $Ph_2P(m\text{-}C_6H_4SO_3Na)$ substitutes all PPh_3 ligands in $Au_{55}(PPh_3)_{12}Cl_6$ and forms $Au_{55}[Ph_2P(m\text{-}C_6H_4SO_3Na)]_{12}Cl_6$. The hydrophilic character of this ligand makes the cluster water soluble.[75] Due to that substitution the stability of the cluster increases. In solution it is completely dissociated into $\{Au_{55}[Ph_2P(m\text{-}C_6H_4SO_3)]_{12}\}^{12-}$ and Na^+.

The study of the degradation of clusters is very informative. This has been investigated intensively on different M_{55} clusters.

DSC measurements on $Au_{55}(PPh_3)_{12}Cl_6$ show a sharp, strong, and exothermic decomposition curve at 156 °C.[76] This thermal decomposition can also be studied in a quantitative preparative scale in solution.

$$Au_{55}(PPh_3)_{12}Cl_6 \xrightarrow{\Delta T} 6(Ph_3P)_2AuCl + 49Au$$

The formation of $(Ph_3P)_2AuCl$ is confirmed by the DSC measurement by a weaker endothermic signal at 201 °C, which is its melting point. The heat of decomposition at 156 °C is 112 J/g or 1590 kJ/Mol of cluster. From these data the approximate nearest-neighbor Au–Au interactions can be estimated. They amount 76.1 kJ, whereas in bulk gold the value is 61.3 kJ. The increased bond strength agrees with EXAFS measurements, which also result in shortened Au–Au distances compared with metallic gold. Although the thermal decomposition gives no information about the degradation mechanism, this is enabled by another degradation reaction. Various M_{55} clusters in dichloromethane solution can be degraded using Pt electrodes to which 20 V dc is applied.[40,77] Obviously by the contact with the positive and negative Pt electrodes the cluster molecules are polarized to such an extent that metal–ligand fragments are separated. Destabilized in such a manner, the complete outer metal shell is lost, leading to the generation of naked M_{13} clusters. They are dense packed like the M_{55} clusters. Their lifetime is long enough to be stabilized by aggregation and form so-called superclusters (clusters of clusters) of the form $[(M_{13})_{13}]_n$. The M_{13} units serve as building blocks for pseudo-close-packed superstructures. X-ray powder diffraction measurements of these metallic looking microcrystalline materials indicate that the M_{13} units are linked via triangular faces. So, multiples of naked M_{13} clusters are formed, which can be regarded as novel metal modifications. However, it turned out that these superclusters are thermodynamically unstable, as they lose their structure in the course of weeks or months at room temperature to give more or less amorphous metal powders. The process of M_{55} cluster degradation and supercluster formation is illustrated in Figure 20. The electrochemical degradation of M_{55} clusters into M_{13} units has recently been confirmed impressively by TOF-SIMS and PDMS investigations on $Au_{55}(PPh_3)_{12}Cl_6$. As these physical methods lead to very important chemical processes, they shall be discussed in this section.[78,79]

Table I. Measured and Calculated Values[a] for the Peak Centers of $(Au_{13})_n^+$ in the Positive SIMS Spectra of $Au_{55}(PPh_3)_{12}Cl_6$

first series			second series			third series		
measd	calcd	n	measd	calcd	n	measd	calcd	n
7 700	7 682	3	12 800	12 803	5	17 900	17 924	7
18 000	17 924	7	22 500	23 045	9	38 400	38 408	15
33 300	33 287	13	43 500	43 530	17	58 900	58 893	23
			84 500	84 499	33	79 400	79 378	31
						99 500	99 862	39
						119 000	120 347	47
						139 000	140 831	55

[a] In unified atomic mass units.

A novel PDMS (plasma desorption mass spectrometry)/SIMS (secondary ion mass spectrometry) combination with a TOF (time of flight) mass spectrometer under kilo- and megaelectronvolt ion impact enables a novel kind of cluster identification and the observation of supercluster formation. In the case of $Au_{55}(PPh_3)_{12}Cl_6$ negative and positive PDMS and SIMS spectra could be registered from samples of different thickness. Surprisingly, all observed mass peaks can be identified as multiples of the Au_{13} unit. In other words, the bombardment of the solid cluster material by Xe^+ ions or fission fragments of a ^{252}Cf source leads to the degradation of the $Au_{55}(PPh_3)_{12}Cl_6$ molecules into Au_{13} units and consequently into smaller metal–ligand fragments, which can be observed in the low-mass range. Table I summarizes the measured and the calculated values for the peak centers.

Three series of SI peaks are observed in the positive spectra. The masses increase with the layer thickness. By PDMS only the first of the three series has been registered. It should be mentioned that the peaks with 33.300 u and 139.000 u correspond to the superclusters $(M_{13})_{13}$ and $(M_{13})_{55}$: magic numbers of magic numbers.

These results agree well with the electrochemical experiments discussed above, although the methods are completely different. They also prove, impressively, that there must be a significant differentiation between surface metal atoms and inner core atoms. The earlier indications, suggesting an electronic separation into outer and inner metal atoms, now are reflected by the degradation behavior of two-shell clusters. Due to these results, ligand-stabilized clusters may possibly be described in such a way that the outer metal shell together with its ligands is regarded as a stabilizing envelope of the real cluster nucleus. Simply expressed, an n-shell ligand-stabilized cluster behaves physically and chemically like a naked $(n - 1)$-shell cluster.

In a broader sense catalytic abilities can also be regarded as chemical properties. However, to describe the catalytic behavior of some investigated clusters, a separate section seems adequate.

IV. Catalysis

The use of large ligand-stabilized transition metal clusters in homogeneous catalysis looks very attractive. Particles in the size range of a few nanometers have not only vertex and edge atoms, but also atoms in faces and therefore they should have all the properties of a supported metal catalyst. However, due to their ligand shell, they become soluble and should be available for homogeneous reactions. A kind of "heterogeneous catalysis in solution"? First attempts with Rh_{55} clusters a few years ago in hydrogenation and hydroformylation reactions with various olefins indeed looked very promising.[80] But, the big disadvantage became evident very quickly: the decomposition of the clusters in solution did not allow any conclusion about the real catalyst. In none of our experiments was the original cluster retained after the reaction. Similar experiences were even made with most of the smaller clusters, which have been used as homogeneous catalysts. The cases, where the original cluster itself can be proved to be working as the catalyst, are insignificant.[81,82] So, whereas the importance of clusters in the homogeneous catalysis has remained low, the number of papers about the successful application of supported clusters and small metal particles is extremely numerous.[68,83-85] Many of these heterogeneous catalysts have become important for industrial processes. The advantage of a heterogeneous catalyst compared with a homogeneous one is clear: it is the simple separation of the products from the catalyst and its repeated use. In contrast, homogeneous catalysts are often characterized by a higher activity and a better selectivity. Mechanistic studies in catalysis have mainly been made on homogeneous catalysts. Mechanisms on an atomic scale in practical heterogeneous catalysis are almost unknown. Model studies under high-vacuum conditions (see for instance[86-89]) give us information about the activities of different faces of monocrystals, edges, terraces, vertices, etc.[90] The varying coordination numbers of the corresponding atoms make catalytic differences clear. Beside numerous modern methods like EXAFS, LEED, UPS, or AES, HRTEM images of clusters and colloids impart impressive knowledge of the atomic processes on metal particles. So, the observation of the behavior of metal clusters and colloids in the microscope led to the finding that especially surface atoms are extremely mobile and that continuous changes of the surface structure happen. These changes become faster, as the particles become smaller. Although the conditions in an electron microscope are very different from those in a reaction vessel, it can be concluded that at elevated temperatures, as corresponding to the conditions of the particles under observation in the electron beam, the surface atoms are highly fluxional. This leads to a continuous renewal of the surface and through this to the catalytic activity. The observations in the microscope under high resolution conditions indicate also that the activity is unequal on different faces. For instance, special activities are observed on (001), (100), (110), and (331) faces, whereas the (111) faces are far less active. These findings agree well with results obtained with model crystallites.

The fixation of catalytically relevant large clusters on a support is, in our experience, subject to two conditions: (1) the ligand must be neutral and may not be substituted with ionic groups like in phen* or $P(m\text{-}C_6H_4SO_3Na)_3$, and (2) the supporting materials must have micropores.

$Rh_{55}[P(t\text{-}Bu)_3]_{12}Cl_{20}$, $Rh_{55}(PPh_3)_{12}Cl_6$, and 30–40-Å Pd clusters with phenanthroline ligands are well suited to be chemisorbed by Na-Y-zeolithe or TiO_2 with micropores. However, the same clusters are almost inactive against Al_2O_3 without micropores or silica.[40,91] BET and DSC measurements and also HRTEM investigations help us to understand these results. One percent solutions of Rh_{55} clusters in dichloromethane are decolorized in a short time if Na-Y-zeolithe or TiO_2 is added. The maximum covering is 5% by weight for the zeolithe and 1.5% by weight for TiO_2. BET measurements on the TiO_2 resulted in a surface of 21 $m^2\ g^{-1}$ with a pore radius of 8.5–10.5 Å. Covered with 1.5% by weight of the cluster, the adsorption capacity is completely lost. This result can only be interpreted in a way that the pore entrances are quantitatively closed by cluster molecules of ca. 20 Å, including the ligand shell. Corresponding conclusions are to be drawn for Na-Y-zeolithe.

DSC measurements on pure $Rh_{55}[P(t\text{-}Bu)_3]_{12}Cl_{20}$ show a sharp, exothermic signal at 110 °C. Na-Y-zeolithe-supported clusters, however, decompose at 200 °C endothermically. This proves that by anchoring the cluster molecules a remarkable stabilization occurs. Another result is noticeable: Na-Y-zeolithe, treated with CH_2Cl_2 shows, after drying at room temperature under vacuum, a broad exothermic signal in the DSC diagram between 150 and 270 °C, indicating the decomposition of CH_2Cl_2 to HCl and carbon or polymeric hydrocarbons. The HCl formation can also be reproduced preparatively. It seems that the presence of crystal water is necessary for that decomposition. If the zeolithe is dehydrated at 400 °C before treating it with CH_2Cl_2, HCl formation cannot be observed. As the DSC measurements show, there is no HCl formation, if the zeolithe is dotted with the cluster material, though the adsorption occurs in CH_2Cl_2. This may indicate that the adsorption of the cluster molecules from solution is faster than the diffusion of CH_2Cl_2 into the micropores.

If cluster-dotted TiO_2 is heated to 200 °C for several hours in vacuum, the following BET measurements

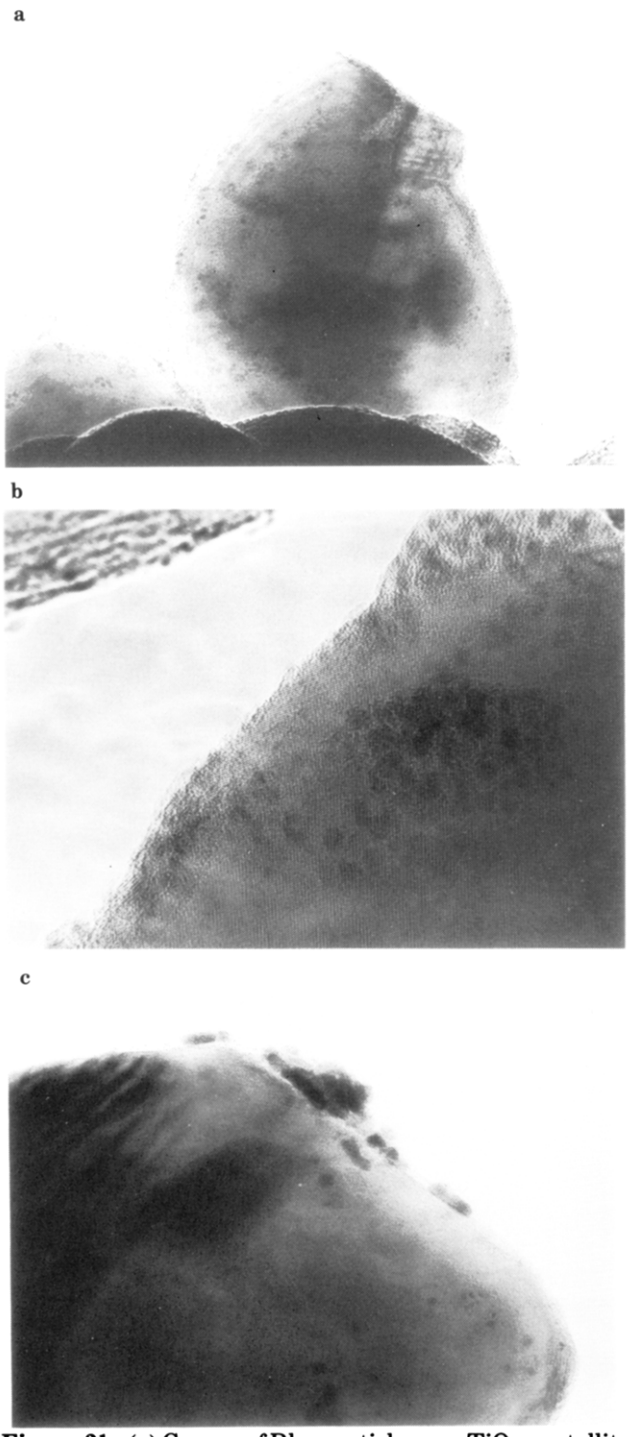

Figure 21. (a) Groups of Rh_{55} particles on a TiO_2 crystallite, (b) a magnified cutout and (c) a cluster dotted TiO_2 crystallite after heating to 200 °C. The cluster molecules formed large aggregates.

shows the complete original activity of adsorption. This means that the cluster molecules have moved from their positions, opening the entrances of the micropores. Indeed, this process can be followed by HRTEM. Figure 21a,b show cluster molecules on TiO_2 crystallites. In 21a it can be recognized that the surface is only very sparsely covered by cluster particles and that the distribution is irregular. Groups of 6–10 molecules can be observed forming islands. van der Waals forces between cluster molecules are probably responsible for the formation of these assemblies. Another interpretation is that the outer field of a micropore entrance has more adsorptive power than other areas.

Figure 21c shows a cluster dotted TiO_2 crystallite after heating to 200 °C. The cluster molecules have left their positions to form large aggregates on the surface. This process demonstrates what has already been indicated by BET and DSC investigations. This finding should be of importance for the application of supported clusters as heterogeneous catalysts, since it has been shown that higher temperatures lead to the decomposition of the original cluster particles.

The use of supported Rh_{55} clusters for hydroformylation reactions is partially promising. During the hydroformylation of ethene at 100 °C and a total pressure of 300 bar without any solvent, a reduction of pressure by 140 bar in the course of 3 h is observed. Repeated increase in pressure leads after 10 h only to a pressure drop of 40 bar, then it remains constant. The fast reaction products are 21% propanol, 48% 2-methyl-2-pentenal, and 28% propionic acid. The deactivation of the catalyst is due to the reaction products, especially to the high boiling, viscous aldol condensation products. Indeed, the lifetime of the catalyst increases remarkable, if it is used in an aqueous suspension, as condensation reactions are suppressed due to the solubility of propanol in water. Between 300 and 100 bar at 100 °C, 290 g of propanol can be prepared, using 1 g of the catalyst (1% weight of cluster). The proportion of aldol condensation products produced under these conditions drops to about 10%. This corresponds to a turnover of 140 $mol_{ethene}\ mol_{Rh}^{-1}\ min^{-1}$, using only the surface Rh atoms for the calculation. No influence on the kind of ligands or the support was observed.

Supported Rh_{55} clusters in aqueous suspension are much more effective if propene is hydroformylated. Pressures between 300 and 100 bar and temperatures between 100–120 °C enabled the production of 3000 g of butanal (n:i = 1:1) by 1.5 g of the catalyst (1% weight of cluster), without any loss of activity. The turnover rate in this case is found to be 400–600 $mol_{propene}\ mol_{Rh}^{-1}\ min^{-1}$. Temperatures > 130 °C lead to a spontaneous deactivation of the catalyst, due to decomposition reactions as discussed above.

All observations support the assumption that these reactions occur heterogeneously. Doubtlessly, the hydroformylation of ethene at least begins heterogeneous under anhydrous conditions. With increasing amounts of organic reaction products, homogeneous catalysis cannot completely be excluded, as rhodium–phosphine fragments might be formed which act as soluble homogeneous catalysts. However, the fact that on the hydroformylation of ethene the activity decreases with increasing concentration of organic products, actually contradicts the presence of soluble catalysts. Additionally, the fact that during the hydroformylation of propene at 130–140 °C the activity drops—although just under these conditions soluble Rh compounds could be formed—supports the assumption that the metal remains on the support.

Hydroformylation reactions with Rh catalysts so far have been exclusively carried out homogeneously. Therefore, direct comparisons with these results do not seem to be useful. However, all things considered it can be stated that homogeneously catalyzed hydro-

Table II. Comparison of Different Pd Catalysts for the Hydrogenation of 1-Hexene[a]

catalyst	Pd/educt ratio (%)	p (bar)	T (°C)	t (min)	products (%)
A	0.012	1	20	360	hexane (100)
B	0.012	1	20	360	hexane (97.2) isomeres (2.8)
C	0.012	1	20	360	hexane (29.7) isomers (21.6) 1-hexene (48.7)

[a] A: 32- and 36-Å Pd clusters *on* TiO_2. B: 32- and 36-Å Pd clusters *in* TiO_2 (prepared by coprecipitation). C: Commercially available Pd catalyst (5% Pd on γ-Al_2O_3, FLUKA).

formylation processes show much better selectivities but much lower turnover frequencies, compared with heterogeneous reactions. Preliminary experiments with liquid alkenes such as hexene or octene indicate that homogeneous reactions are favored, as soluble rhodium phosphine complexes are found in solution, leading to catalytically active product solution.

Hydrogenation reactions with supported Pd clusters are definitely heterogeneous. The 30–40-Å Pd clusters, described in section 2, mainly consist of seven- and eight-shell particles and are stabilized by phenanthroline and oxygen. These can easily be anchored on TiO_2 from a pyridine–water mixture.[40] As is known from investigations of $Pt_{309}phen^*_{36}O_{30}$, such oxygen covered complexes can be deoxygenated by hydrogen.[92] One can conclude that such a deoxygenation reaction can also occur with the Pd particles in the course of a hydrogenation reaction. Consequently, one can assume that oxygen-free Pd clusters on TiO_2, only coordinated by phenanthroline, act as catalysts. After numerous applications in hydrogenation reactions the catalysts do not show any reduction of their activity. As product solutions are absolutely inactive, one can be sure that the reactions are heterogeneous. Table II summarizes the results of the hydrogenation reaction of 1-hexene with three kinds of catalysts: the catalyst with Pd clusters anchored *on* TiO_2 (A), a catalyst with Pd clusters incapsulated *in* TiO_2 (B) (prepared by coprecipitation of TiO_2 with cluster material from aqueous solution), and a commercially available Pd catalyst[40] (C).

A possible advantage of catalysts with 30–40-Å clusters, compared with a conventional catalyst can be expected due to the small size distribution. The methods to prepare the usual metal catalysts consist in the reduction of metal salts on a support, yielding particles with a size distribution. Although we do not use completely uniform clusters in this case, the major part of the cluster molecules is between 30–40 Å, i.e. a very narrow region. As can be seen in the 1-hexene case, the hydrogenation at normal pressure and at room temperature gives 100% hexane. The commercial Pd catalyst forms, under identical conditions and during the same time, only 29.7% hexane and 21.6% hexene isomers; 48.7% is isolated as unchanged 1-hexene.

The availability of water-soluble clusters opens a series of novel applications, for instance the synthesis of modified catalysts: e.g. from titanium acid esters, TiO_{aq} can be precipitated in the presence of clusters. After drying, the cluster molecules are uniformly dispersed in the TiO_2 particles. As a hydrogenation reaction of 1-hexene shows, such a catalyst has approximately the same activity as the catalyst formed by surface adsorbed clusters. Under the same conditions, 97.2% of hexane is formed. In fact, the activity is higher, when the number of available cluster molecules on the surface becomes smaller, as most of them are incapsulated. The advantage of such a catalyst is its lifetime. Destroyed surfaces are continuously substituted by deeper lying fresh material. The use of such catalysts could be of interest, when strong mechanical strain can be expected as is the case in the automobile exhaust gas purification.

Table III. Hydrogenation Reactions of Alkenes and 1-Hexyne with 32- and 36-Å Pd Clusters on TiO_2 (Catalyst A)

olefin	Pd/ olefin	p (bar)	T (°C)	t (min)	products (%)
1-hexene	0.012	1	20	360	hexane (100)
1,3-COD	0.010	1	30	300	cyclooctene (100)
cyclooctene	0.010	1	100	240	cyclooctane (100)
dicyclopentadiene	0.009	1	105	280	dicyclopentene (96.2)
		1	105	420	dicyclopentane (98.9)
acrolein	0.008	100	55	11	propanal (100)
crotonaldehyde	0.008	220	85	60	butanal (95.1)
1,4-cyclohexadiene	0.010	1	80	450	cyclohexane (99.8)
		100	50	23	cyclohexane (98.0)
1,3-cyclohexadiene	0.010	100	50	16	cyclohexene (85.9) cyclohexane (13.7)
1-hexyne	0.035	1	20	180	1-hexene (97.5) hexane (2) isomers (0.5)

Table III contains the results of some hydrogenation reactions of alkenes and hexyne, studied up to date. Selective hydrogenations, observed in some cases, may be of special interest.

1-Hexyne is hydrogenated under mild conditions to 1-hexene. 1,3-Cyclooctadiene can be hydrogenated at 1 bar and 30 °C in 100% yield to cyclooctene. At 220 bar and 70 °C it is transformed quantitatively to cyclooctane. Dicyclopentene is formed from dicyclopentadiene at 1 bar and 105 °C with 36.2% yield in the course of 280 min. After 420 min a quantitative yield of dicyclopentane was observed.

At present it looks as if transition metal clusters, anchored on supports or incapsulated in supports could become valuable catalysts with interesting properties. These have several improvements over conventional catalysts. Especially the embedding of water-soluble, air-stable clusters in ceramic materials gives products which have promising properties.

V. Ligand-Stabilized Clusters as Molecular Devices

As already mentioned in the introduction, ligand-stabilized metal clusters are promising candidates for the application as quantum dots. The new physical properties which are to be expected in comparison with the bulk on the one side and with the molecular state on the other side, are exclusively controlled by quantum mechanical conditions. The so-called size-induced metal-insulator transition (SIMIT), defined by Nimtz,[93] is already valid for 20-nm particles. Due to this quantization effect, standing electron-waves with discrete energy levels are formed. All presently known results of conductivity measurements on concentrated ligand-stabilized transition metal clusters prove an intercluster tunnel conductivity. Figure 22 shows the conductivity σ_{DC} of $Au_{55}(PPh_3)_{12}Cl_6$ and $Pd_{561}phen_{36}O_{200}$

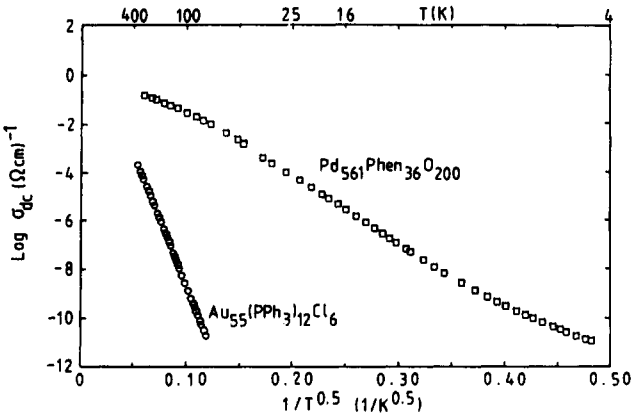

Figure 22. σ_{DC} as a function of $T^{-1/2}$ for $Au_{55}(PPh_3)_{12}Cl_6$ and $Pd_{561}phen_{36}O_{200}$.

in dependence of temperature.[94] As could be expected, the conductivity increases with increasing temperatures. Secondly, the temperature dependence of the smaller Au_{55} cluster is significantly more pronounced than for Pd_{561}. However, these conductivity measurements do not show any indication for the separation of inter- and intracluster effects. The impedance spectroscopy (IS) has become a convenient method to study different materials in order to combine macroscopic properties and atomic processes. Fitting, simulation, and evaluation programs which have been developed during the last few years helped to interpret the fine structure of immittance spectra.[95] The low-frequency IS has become an excellent method to describe different processes in materials science. It has not only been used to understand ionic relaxation processes ("hopping ions"), e.g. in interface layers or in solid matrixes, even electronic relaxation processes at lower frequencies seem to become a domain of this method. Hopping electrons and localized electrons in traps have been known from semiconductor–insulator interfaces or from metal–insulator materials and glasses. The conduction behavior of $Au_{55}(PPh_3)_{12}Cl_6$ in a pellet has been described using such models.[96] However, to explain the "quantum-dot behavior" of e.g. Au_{55} clusters, the intracluster properties such as activation enthalpies and relaxation frequencies must be investigated.

Due to their ligand shells, the single Au_{55} cluster nuclei cannot coalesce. Disks with a diameter of 5 mm and a thickness of 0.2–0.4 mm have been produced by a pressing power of 2.5×10^8 Pa. The gravimetrically determined density of 3.37 g/cm^3 shows that an almost-perfect close-packed arrangement has been reached, the density of which is calculated to be 3.704 g/cm^3. Figure 23 shows the Argand diagram of the impedance Z^* of a $Au_{55}(PPh_3)_{12}Cl_6$ pellet under nitrogen at 293 K.

The numbers along the plot indicate the logarithm of the measuring frequency ν. The semicircles result form the best data fit and can be understood as an ideal Debye resistance (R_2)/capacity (C_2) link (low-frequency process 2) and in addition a Cole–Cole resistance (R_1)/CPE (constant-phase element) link (higher frequency process 1). It results in the fact that the Ohmic part is the same for both relaxation processes ($R_1 \approx R_2$; $R_{total} = 2R_1$). However, the relaxation frequencies differ by a factor 2. As the basic processes are thermally activated, the activation enthalpies for the Debye relaxation process EA_2 has been calculated to be 0.16

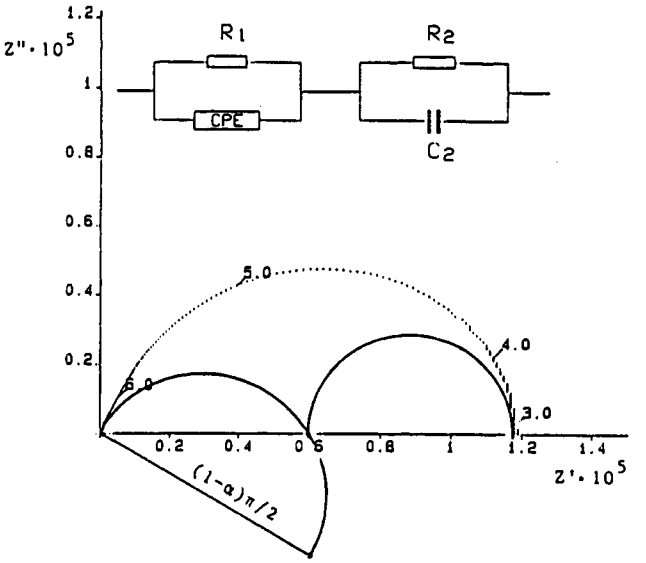

Figure 23. Unscaled Argand diagram of compact $Au_{55}(PPh_3)_{12}Cl_6$ at 293 K. The numbers along the plot indicate the logarithm of the measuring frequency ν. Above a circuit equivalent for the electric response of the sample. Below the measured plot are the Argand circles belonging to each separate link.

± 0.03 eV. For the Cole–Cole process EA_1 is 0.15 ± 0.03 eV. So, within the experimental error it is $EA_2 \approx EA_1$. As the relaxation times τ_1 and τ_2 and the resistances R_1 and R_2 show the same Arrhenius behavior, the capacitances C_2 and CPE must be independent of temperature.

As a consequence of these results, two different conductivity processes can be concluded (from R_{total} and R_2), namely one with the specific conductivity $\sigma_{total} = 1.61 \times 10^{-4}$ ohm^{-1} m^{-1} and the other with $\sigma_2 = 3.23 \times 10^{-4}$ ohm^{-1} m^{-1}.

These conductivities can only be caused by electronic processes. In previous papers[96] the electronic overall conductivity has been discussed as a consequence of stochastic multiple-site hopping processes. Beginning intercluster effects, caused by electron tunneling between neighboring clusters, has already been subject for the discussion. Now, the higher frequency Cole–Cole process 1 is to be interpreted as a pair relaxation (two-site process), whereas the Debye process 2 must be discussed as a preceding intracluster step. Both processes are, of course, coupled in concentrated samples such as pellets.

The Au_{55} nucleus is a naturally built quantum box. In agreement with quantum mechanics this cluster contains some free electrons, coming from the 1g orbitals of the Au_{55} core in agreement with the so-called jellium model. Electrons in such a quantum box are localized both geometrically as well as quantum mechanically. They form wave packets with a maximum wavelength of $\lambda = 2x$. Smaller quantum dots could only contain higher energetic free electrons and should be unstable. The Au_{55} quantum box has a minimum size in which the last free electrons are fenced: *Au_{55} is one of the last metals.* The lateral extension of x is given by the known relationship for a 3D electron gas:

$$x = \hbar\pi(2mE_F)^{-1/2}$$

where m = electron mass and E_F = Fermi energy. Due to the Pauli principle the number N_{ex} of electronic

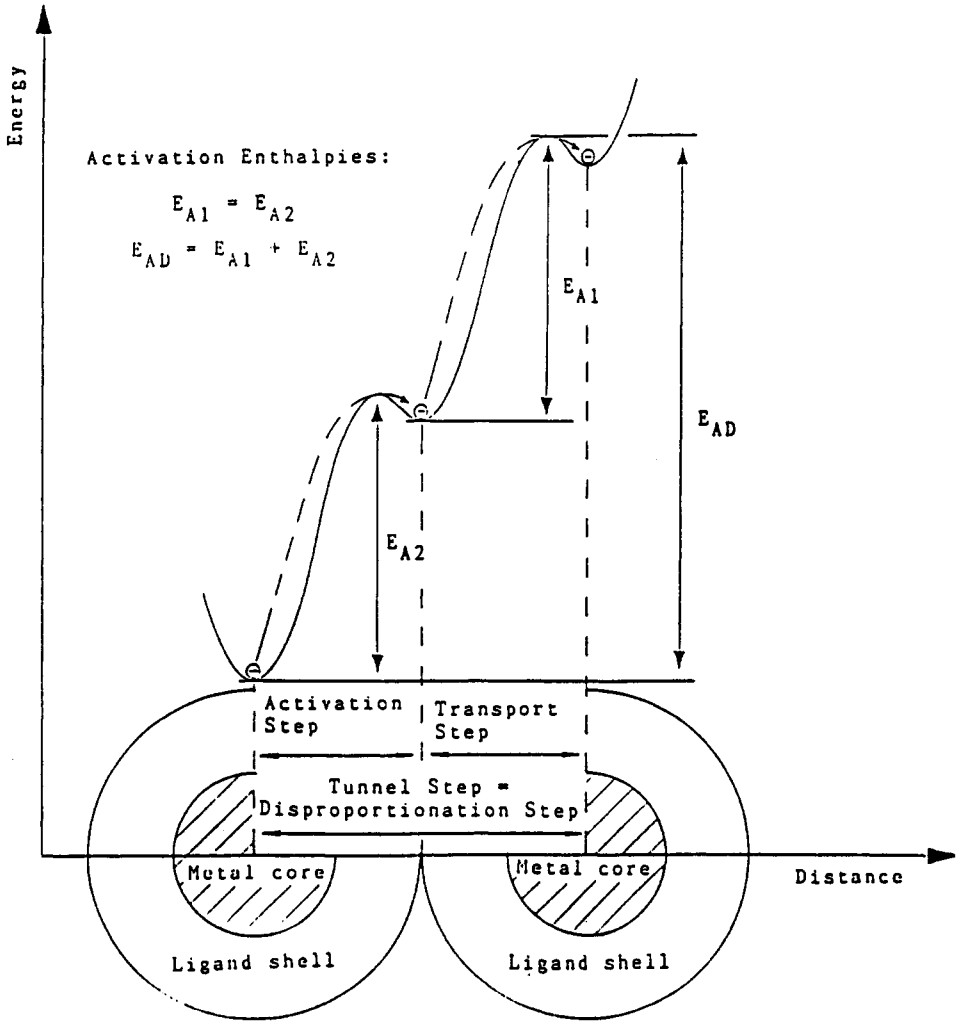

Figure 24. Potential profile for a cluster pair. Activation step and transport steps cause the tunnel step (activation enthalpy EA_D).

states, participating in the resonance process is 1 *or* 2 with energies $E_{ex1/2}$, known from the experimentally determined density of electronic states $D_{ex} \approx 10.75\ eV^{-1}$, assuming an approximately closest sphere packing of the Au_{55} clusters within the pellet:

$$E_{ex1} = 0.093\ eV = E_{F1} \rightarrow x_1 = 2.01\ nm$$

$$E_{ex2} = 0.186\ eV = E_{F2} \rightarrow x_2 = 1.45\ nm$$

So, there remain only two possibilities to describe the electronic state in $Au_{55}(PPh_3)_{12}Cl_6$: a double occupied cluster core with a 1.45-nm diameter or a single occupied particle with an approximate 2.01-nm diameter. As the Au_{55} cluster core has a diameter 1.4 nm it follows that it contains two free electrons with a Fermi energy of $E_F = 0.19$ eV in the ground state. These results have been gained by the only assumption that the samples used for the measurements contain an approximate close-packed structure, what is indeed almost completely the case, as the density measurements proved. The cluster diameter x of 1.45 nm results independent on any other presumptions.

The Debye relaxation time $\tau_2 = R_2 \times C_2 \approx 2.6 \times 10^{-6}$ s is determined by the intracluster conductivity of the Au_{55} cluster, caused by two "free metallic" electrons, and the capacitance C_2, which is defined by the structure and the polarizability of the ligand shell.

This capacitance C_2 enables the measurement of the energy which is necessary for the polarization of the ligand shell as a consequence of the hopping of an electron to a point, where it decides to either remain within the same cluster or to tunnel into the neighboring cluster molecule. Therefore, the relaxation of the ligand shell is the reason for the observed frequency dependence.

The Cole–Cole relaxation time at 293 K is $\tau_1 = 1.3 \times 10^{-6}$ s. It lies at higher frequencies by the factor 2 and is determined by the intracluster conductivity ($R_1 = R_2$) and the capacitance CPE between the clusters.

Figure 24 elucidates the relationship between activation enthalpies and tunneling steps. Activation and transport steps cause the tunneling step.

In Figure 25 the most important result of the discussed measurements and relationships is shown: the total conductivity σ_{total} is doubled under resonance conditions to $\sigma_1 = \sigma_2 = 2\sigma_{total}$. In other words, under resonance conditions two $Au_{55}(PPh_3)_{12}Cl_6$ cluster molecules can be used as a molecular switch.

The preceding discussion of results led to a detailed idea of the electronic structure of 1–2-nm quantum dots. The quantum size effect causes the last metallic electrons to be localized in a quantum box of the lateral dimension of the cluster and to be freely mobile. The realization of such a quantum dot only depends on the

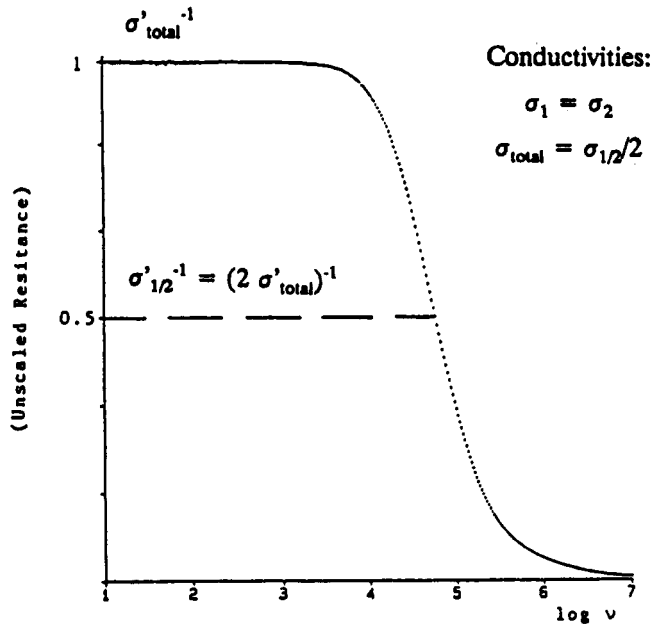

Figure 25. A sequence of activation and transport step leads to a total conductivity σ_{total} which is *doubled* under resonance conditions.

fact if the binding energy of these electrons exceeds or not the de Broglie energy. This leads to the conclusion that clusters of the type of $Au_{55}(PPh_3)_{12}Cl_6$ can be used as quantum devices with at least one "molecular orbital" occupied by two such electrons.

Pellets of $Au_{55}(PPh_3)_{12}Cl_6$, pressed with contacting gold foils, are already a handy device with typical electronic quantum properties. Due to the densest packed cluster molecules under resonance conditions a pack of quantum channels with ca. 2-nm diameter (cluster nucleus + ligand shell) is produced. In Figure 26a such a quantum channel is shown symbolically. Figure 26b elucidates the construction of a pellet of channels. Such a pellet can be regarded as a tunneling resonance resistance (TRR), the total resistance of which can be bisected by a resonance frequency of 60 kHz at ambient temperatures.

A $Au_{55}(PPh_3)_{12}Cl_6$ pellet can additionally be regarded as a cellulary automate with contacts only at the marginal points, in which each quantum dot (cluster molecule) corresponds to 12 neighbors. One cubic centimeter of densest packed cluster molecules contains about 10^{20} quantum dots; a pellet with a 1-cm^2 surface contains about 10^{13} quantum channels. The magic number of 250 nm for structural elements in the nanotechnique[96] is now reduced to about 4 nm for two quantum dots (see Figure 26a). Three dimensionally, this corresponds with a reduction of approximately 4×10^{-6}!

VI. Conclusions

The transition from the bulk to the molecular state is characterized by an important range where, due to the lack of marked properties of the one as well as of the other species, completely novel properties can be expected. These nanostructured species serve as objects of study in chemistry and in physics, respectively. From metal clusters, chemistry expects interesting reactions, especially in catalysis. Nanosized metal particles offer physics ideal systems for the investigation of various fundamental effects. However, ahead of all possible investigations there is the preparative hurdle to overcome. Ideal systems for chemistry and physics would consist of uniform, crystalline, and undisturbed (e.g. by ligands) metal particles in the range between 1 and about 100 nm. In spite of different tricky methods to generate such naked clusters, their application is restricted as they cannot be isolated in a preparative scale. Consequently, more or less all studies concentrate on the synthesis of well-defined ligand stabilized clusters and, in a reduced manner, also on ligand stabilized

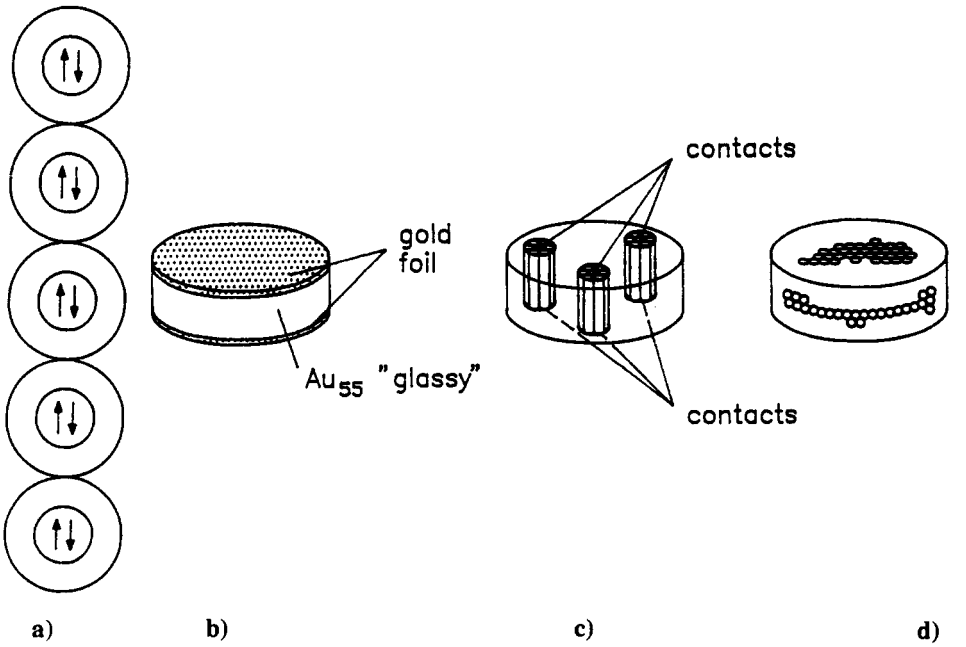

Figure 26. (a) Quantum channel of Au_{55} clusters (section of the closest sphere packing in a glassy sample) at/above resonance frequency and (b) disk of pressed $Au_{55}(PPh_3)_{12}Cl_6$ cluster molecules which may be contacted facially by gold foils to build up a tunnel resonance resistance. It can also be contacted by microscopic scanning patterns in the dimension of single quantum channels (c) or facially and laterally to give a cellulary automate (d).

colloids. Indeed, nowadays we are able to stabilize mono- or bimetallic colloids to such an extent that they can not only be isolated in solid state, but can also be redispersed in any concentration. This enables a new quality of investigations of colloids. Such colloids differ principally from the known matrix isolated colloids where the main part of the mass consists of the matrix material. Colloids, coordinated by $P(m\text{-}C_6H_4SO_3Na)_3$ or $p\text{-}H_2N\text{-}C_6H_4SO_3Na$ are covered by only a thin but strongly fixed skin, preventing coalescence.

On the way to smaller particles we find a palladium species in the 3–4-nm range, consisting of mainly two different kind of clusters, namely those with 3.2-nm and those with 3.6-nm diameters. The ligand shell consists of phenanthroline molecules and of oxygen. Presently, they can be regarded as the largest clusters with satisfying characterization or as very small colloids with an extremely narrow particle-size distribution. These palladium clusters are useful objects for studies in heterogeneous catalysis. The importance of such clusters is not only to be seen in the goal to explore novel and better catalysts, but to help for a better understanding of catalytic processes. Modern high-resolution electron microscopy, linked with the involved analytical facilities enables nowadays the exact characterization of these nanoscaled particles before their chemical application, due to their preparative availability.

The monodisperse character of metal clusters leads to markedly increased reaction rates, as could be observed for hydroformylation and hydrogenation reactions. The use of ligand-stabilized, supported metal clusters is just at a very first but promising beginning. The reduction of metal particles to the size range of 2.5–1.5 nm finds an increasing interest in physics, as we get closer to the area where the disappearance of typical metal properties, that is the decrease of freely mobile electrons, is proceeded to such an extent that quantum size effects can be expected. The cluster molecule $Pt_{309}phen^*_{36}O_{30}$ shows two different kind of Pt atoms in the ^{195}Pt NMR spectrum. Besides a signal which is typical for ligand-coordinated surface atoms, a second signal with a remarkable Knight shift, similarly observed in bulk platinum, is registered. This signal is caused by the inner cluster nucleus, consisting of 147 atoms. It contains still so many freely mobile electrons that metallic-like behavior results.

In $Au_{55}(PPh_3)_{12}Cl_6$ with a cluster nucleus of 1.4 nm in diameter the existence of *two last freely mobile electrons* could be proven. So, with about 50 atoms we have definitely reached the borderline of the metallic state! These two "last metallic" electrons lead to consequences which cannot be completely estimated concerning their future importance. As the Au_{55} nuclei in solid samples are separated by the ligand shell from each other, these two electrons can only become mobile *between* the clusters by activation. Because this activation energy corresponds to definite values, a sample of closest packed $Au_{55}(PPh_3)Cl_6$ molecules is nothing but a system of parallelly ordered quantum wires under resonance conditions (tunnel resonance resistance, TRR). If the interaction of each cluster with its 12 neighbors occurs, such a pellet can also be regarded as a cellulary automate. The density of electronic switches has, compared with common semiconductors, raised to a factor of 10^5–10^6!

By this device a breakthrough in microelectronics might have succeeded. The consequences of these findings are still unpredictable. After a lot of premature praise, metal clusters beginning to be established in chemistry and physics as building blocks of the future.

VII. References

(1) Wang, Y.; Herron, N. *J. Phys. Chem.* **1987**, *91*, 257.
(2) Bawendi, M. G.; Steigerwald, M. L.; Brus, L. E. *Annu. Rev. Phys. Chem.* **1990**, *41*, 477.
(3) Kortan, A. R.; Hull, R.; Opila, R. L.; Bawendi, M. G.; Steigerwald, M. L.; Carroll, P. J.; Brus, L. E. *J. Am. Chem. Soc.* **1990**, *112*, 1327.
(4) Steigerwald, M. L.; Brus, L. E. *Acc. Chem. Res.* **1990**, *23*, 183.
(5) Fojitk, A.; Weller, H.; Koch, U.; Henglein, A. *Ber. Bunsen-Ges. Phys. Chem.* **1984**, *88*, 969.
(6) Jewell, J. J.; Harbison, J. P.; Scherer, A.; Lee, Y. H.; Florez, L. T. *IEEE J. Quantum Electron.* **1991**, *27*, 1332.
(7) *The Technology and Physics of Molecular Beam Epitaxy*; Parker, E. H. C., Ed.; Plenum Publishing: New York, 1985.
(8) Simon, U.; Schmid, G.; Schön, G. *Angew. Chem., Int. Ed. Engl.*, in press.
(9) Hayat, M. A. *Collodial Gold, Principles, Methods and Applications*; Academic Press: New York, 1989; Vol. 1.
(10) Hirau, H.; Nakao, Y.; Toshima, N. *J. Macromol. Sci. Chem.* **1979**, *A13*, 633.
(11) Hirau, H.; Nakao, Y.; Toshima, N. *J. Macromol. Sci. Chem.* **1979**, *A13*, 727.
(12) Hirau, H.; Nakao, Y.; Toshima, N. *J. Macromol. Soc. Chem.* **1979**, *A13*, 1117.
(13) Meguro, K.; Nakamura, Y.; Hayashi, Y.; Torizuka, M.; Esumi, K. *Bull. Chem. Soc. Jpn.* **1988**, *61*, 347.
(14) Komiyama, M.; Hirai, H. *Bull. Chem. Soc. Jpn.* **1983**, *56*, 2833.
(15) Yonezawa, Y.; Sato, T.; Ohno, M.; Hada, H. *J. Chem. Soc., Faraday Trans. 1* **1987**, 1559.
(16) Larpent, C.; Patin, H. *J. Mol. Catal.* **1988**, *44*, 191.
(17) Turkevich, J.; Stevenson, P. C.; Hillier, J. *Disc. Faraday Soc.* **1951**, *11*, 55.
(18) Mabuchi, M.; Takenaka, T.; Fujiyoshi, Y.; Uyeda, N. *Surf. Sci.* **1982**, *119*, 150.
(19) Frens, G. *Kolloid Z. Z. Polym.* **1972**, *250*, 736.
(20) Duff, D. G.; Curtis, A. C.; Edwards, P. P.; Jefferson, D. A.; Johnson, B. F. G.; Logan, D. E. *Angew. Chem., Int. Ed. Engl.* **1987**, *26*, 676.
(21) Duff, D. G.; Curtis, A. C.; Edwards, P. P.; Jefferson, D. A.; Johnson, B. F. G.; Logan, D. E. *J. Chem. Soc., Chem. Comm.* **1987**, 1264.
(22) Freund, P. L.; Spiro, M. *J. Phys. Chem.* **1985**, *89*, 1074.
(23) Westerhausen, J.; Henglein, A.; Lilie, J. *Ber. Bunsen-Ges. Phys. Chem.* **1981**, *85*, 182.
(24) Zsigmondy, R.; Thiessen, P. A. *Das kolloidale Gold*; Akademische Verlagsgesell-schaft: Leibzig, 1925.
(25) Schmid, G.; Lehnert, A. *Angew. Chem., Int. Ed. Engl.* **1989**, *28*, 780.
(26) Schmid, G.; Lehnert, A.; Kreibig, U.; Adamczyk, Z.; Belouschek, P. *Z. Naturforsch.* **1990**, *45b*, 989.
(27) Houben-Weyl. *Methoden der Organischen Chemie*; Thieme-Verlag: Stuttgart, 1955; Vol. 9.
(28) Malm, J.-O.; Bovin, J.-O.; Schmid, G. Unpublished results.
(29) Boese, R.; Schmid, G. Unpublished results.
(30) Turkevich, J.; Kim, G. *Science* **1970**, *169*, 873.
(31) Rampino, L. D.; Nord, F. F. *J. Am. Chem. Soc.* **1941**, *63*, 2745.
(32) Meguro, K.; Torizuka, M.; Esumi, K. *Bull. Chem. Soc. Jpn.* **1988**, *61*, 341.
(33) Kiwi, J.; Kalyanasundaram, K.; Grätzel, M. *Struct. Bonding* **1982**, *49*, 37.
(34) Furlong, D. N.; Launikonis, A.; Sasse, W. H. F. *J. Chem. Soc., Faraday Trans. 1* **1984**, *80*, 571.
(35) Miner, R. S., Jr.; Namba, S.; Turkevich, J. In *Proceedings of the VII International Congress on Catalysis*; Seiyama, T., Tanabe, K., Eds.; Elsevier: New York, 1981.
(36) Marzke, R. F.; Glaunsinger, W. S.; Bayard, M. *Solid State Commun.* **1976**, *18*, 1025.
(37) Michel, J. B.; Schwartz, J. T. *Studies Surf. Sci. Catal.* **1987**, *31*, 669.
(38) Schmid, G.; Lehnert, A.; Malm, J.-O.; Bovin, J.-O. *Angew. Chem., Int. Ed. Engl.* **1991**, *30*, 852.
(39) Jefferson, D. A. Unpublished results.
(40) Schmid, G.; Harms, M. *J. Am. Chem. Soc.*, in press.
(41) Schmid, G. *Polyhedron* **1988**, *7*, 2321.
(42) Schmid, G. *Mater. Chem. Phys.* **1991**, *29*, 133.
(43) Vargaftik, M. N.; Zagarodnikov, V. P.; Stolyarov, I. P.; Moiseev, I. I.; Likhobolov, V. I.; Kochubey, D. I.; Chuvilin, A. L.; Zaikowsky, V. I.; Zamaraev, K. I.; Timofeeva, G. I. *J. Chem. Soc., Chem. Commun.* **1985**, 937.
(44) Schmid, G.; Morun, B.; Malm, J.-O. *Angew. Chem., Int. Ed. Engl.* **1989**, *28*, 778.

(45) Schmid, G.; Boese, R.; Pfeil, R.; Bandermann, F.; Meyer, S.; Calis, G. H. M.; van der Velden, J. W. A. *Chem. Ber.* **1981**, *114*, 3634.
(46) Schmid, G.; Giebel, U.; Huster, W.; Schwenk, A. *Inorg. Chim. Acta* **1984**, *85*, 97.
(47) Schmid, G.; Huster, W. *Z. Naturforsch.* **1986**, *41b*, 1028.
(48) Schmid, G. *Endeavour* **1990**, *14*, 172.
(49) Wieringa, H. A.; Soethout, C. C.; Gerritsen, J. W.; van de Leemput, L. E. C.; van Kempen, H.; Schmid, G. *Adv. Mater.* **1990**, *2*, 482.
(50) van de Leemput, L. E. C.; Gerritsen, J. W.; Rongen, P. H. H.; Smokers, R. T. M.; Wieringa, H. A.; van Kempen, H.; Schmid, G. *J. Vac. Sci. Technol.* **1991**, *B9*, 814.
(51) Becker, C.; Fries, Th.; Wandelt, K.; Kreibig, U.; Schmid, G. *J. Vac. Sci. Technol.* **1990**, *B9*, 810.
(52) Fries, Th.; Wandelt, K.; Schmid, G.; Boese, R.; Fauth, K. Unpublished results.
(53) Teo, B. K.; Shi, X.; Zhang, H. *J. Am. Chem. Soc.* **1992**, *114*, 2743.
(54) Teo, B. K.; Zhang, H. *Angew. Chem., Int. Ed. Engl.*, in press.
(55) Fenske, D.; Ohmer, J.; Hachgenei, J.; Merzweiler, K. *Angew. Chem., Int. Ed. Engl.* **1988**, *27*, 1277.
(56) Fenske, D.; Krautscheid, H. *Angew. Chem., Int. Ed. Engl.* **1990**, *29*, 1452.
(57) Fenske, D.; Fleischer, H.; Persau, C. *Angew. Chem., Int. Ed. Engl.* **1989**, *28*, 1665.
(58) Fenske, D.; Persau, C. *Z. Anorg. Allg. Chem.* **1991**, *593*, 61.
(59) Chini, P. *J. Organomet. Chem.* **1980**, *200*, 37.
(60) Ceriotti, A.; Demartin, F.; Longoni, G.; Manassero, M.; Marchionna, M.; Piro, G.; Sansoni, M. *Angew. Chem., Int. Ed. Engl.* **1985**, *24*, 697.
(61) Ozin, G. A.; Mitchell, S. A. *Angew. Chem., Int. Ed. Engl.* **1983**, *22*, 674.
(62) Morse, M. D. *Chem. Rev.* **1986**, *86*, 1049.
(63) Schumacher, E. *Chimia* **1988**, *no. 11*, 357.
(64) Kappes, M. *Chem. Rev.* **1988**, *88*, 369.
(65) Smit, A. H. A.; Thiel, R. C.; de Jongh, L. J.; Schmid, G.; Klein, N. *Solid State Commun.* **1988**, *65*, 915.
(66) Fairbanks, M. C.; Benfield, R. E.; Newport, R. J.; Schmid, G. *Solid State Commun.* **1990**, *73*, 431.
(67) Marcus, M. A.; Andrews, M. P.; Zegenhagen, J.; Bommannavar, A. S.; Montano, P. *Phys. Rev.* **1990**, *B42*, 3312.
(68) de Jongh, L. J.; Baak, J.; Brom, H. B.; van der Putten, D.; van Ruitenbeek, J. M.; Thiel, R. C. *Proceedings Int. Symp. on Physics and Chemistry of Finite Systems: From Clusters to Crystals*; NATO ASI Series, Richmond 1991, Plenum: New York, 1991.
(69) de Jongh, L. J.; Brom, H. B.; Longoni, G.; Pronk, B. J.; Schmid, G.; van Staveren, M. P. J. *J. Chem. Res.* **1987**, 150.
(70) de Jongh, L. J.; de Aguiar, J. A. O.; Brom, H. B.; Longoni, G.; van Ruitenbeek, J. M.; Schmid, G.; van Staveren, M. P. J.; Thiel, R. C. *Z. Phys. D.* **1989**, *12*, 445.
(71) Rösch, N.; Ackermann, L.; Paccioni, G. *J. Am. Chem. Soc.* **1992**, *114*, 3549.
(72) Kreibig, U.; Fauth, K.; Granqvist, C.-G.; Schmid, G. *Z. Phys. Chem.* **1990**, *169*, 11.
(73) Fauth, K.; Kreibig, U.; Schmid, G. *Z. Phys. D* **1991**, *20*, 297.
(74) Schmid, G. *Struct. Bonding* **1985**, *62*, 51.
(75) Schmid, G.; Klein, N.; Korste, L.; Kreibig, U.; Schönauer, D. *Polyhedron* **1988**, *7*, 605.
(76) Benfield, R. E.; Creighton, J. A.; Eadon, D. G.; Schmid, G. *Z. Phys. D* **1989**, *12*, 533.
(77) Schmid, G.; Klein, N. *Angew. Chem., Int. Ed. Engl.* **1986**, *25*, 922.
(78) Feld, H.; Leute, A.; Rading, D.; Benninghoven, A.; Schmid, G. *J. Am. Chem. Soc.* **1990**, *112*, 8166.
(79) Feld, H.; Leute, A.; Rading, D.; Benninghoven, A.; Schmid, G. *Z. Phys. D* **1990**, *17*, 73.
(80) Schmid, G. *Aspects Homogeneous Catal.* **1990**, *7*, 1.
(81) Markó, L.; Vizi-Orosz, A. In *Stud. Surf. Sci. Catal.* **1986**, *29*, 89.
(82) Walther, B. *Z. Chem.* **1989**, *29*, 117.
(83) Gates, B. C. In ref 68, p 514.
(84) Psaro, R.; Ugo, R. In ref 68, p 427.
(85) Knözinger, H.; Gates, B. C. In ref 68, p 531.
(86) Muetterties, E. L. *Angew. Chem., Int. Ed. Engl.* **1978**, *17*, 545.
(87) Ertl, G. *Stud. Surf. Sci. Catal.* **1986**, *29*, 577.
(88) Hiemenz, P. C. *Principle of Colloid and Surface Chemistry*, 2 ed., Dekker, M., Inc.: New York, 1980.
(89) van Hardeveld, R.; van Montfoort, A. *Surface Sci.* **1966**, *4*, 396.
(90) Somorjai, G. A. *Acc. Chem. Res.* **1976**, *9*, 248.
(91) Schmid, G.; Küpper, R.; Hess, H.; Malm, J.-O.; Bovin, J.-O. *Chem. Ber.* **1991**, *124*, 1889.
(92) Morun, B. Thesis, University of Essen, 1989.
(93) Nimtz, G.; Marquard, P.; Gleiter, H. *J. Cryst. Growth* **1988**, *86*, 66.
(94) Brom, H. B.; van Staveren, M. P. J.; de Jongh, L. J. *Z. Phys. D* **1991**, *20*, 281.
(95) Macdonald, J. R. *Impedance Spectroscopy*; Wiley and Sons: New York, 1987; p 246.
(96) Corcoran, E. *Spekt. Wissenschaft* **1991**, January, 76.